Review | Open Access

Energy Materials

Yasin *et al. Energy Mater.* **2026**, *6*, 600093 **DOI:**10.20517/energymater.2026.38

Research progress of phosphorus-carbon composites as anode materials for lithium-ion batteries

Adan Yasin[1,2,#], Qingsheng Chen[1,2,#], Jiawei Wan[1,2], Nan Xu[1,2], Peng Peng[2], Zijian Zheng[3], Jiangyan Wang[1,2,*]

Keywords:
Phosphorus carbon composites, lithium-ion batteries, anode materials, electrochemical performance

Citation: Yasin, A.; Chen, Q.; Wan, J.; Xu, N.; Peng, P.; Zheng, Z.; Wang, J. Research progress of phosphorus-carbon composites as anode materials for lithium-ion batteries. *Energy Mater.* **2026**, *6*, 600093. https://dx.doi.org/10.20517/energymater.2026.38

Received: 22 Mar 2026
First Decision: 12 May 2026
Revised: 1 Jun 2026
Accepted: 16 Jun 2026
Published: 4 Aug 2026

Academic Editors: Zhipeng Sun, Federico Bella
Copy Editor: Fangling Lan
Production Editor: Fangling Lan

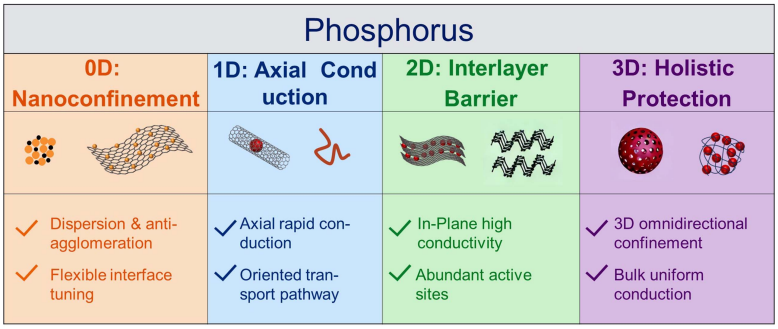

Abstract

Research on high-performance anodes other than graphite has been accelerated with the increasing demand for advanced lithium-ion batteries. Phosphorus-based anodes, including black phosphorus and red phosphorus, possess a high theoretical capacity, but there are intrinsic limitations, including severe volume changes, low electrical conductivity, and unstable cycling stability. This mini-review focuses on the latest developments in solving the above problems by designing phosphorus-carbon composites with different dimensionalities, from zero-dimensional quantum dots and one-dimensional carbon nanotube hybrids to two-dimensional graphene and three-dimensional sponges. Moreover, the intrinsic mechanisms behind the performance improvement in phosphorus-carbon composites with different dimensionalities are deeply discussed in this review. Furthermore, the unique challenges and recent progress of phosphorus-carbon anodes in all-solid-state batteries are also discussed, comparing their degradation mechanisms with conventional liquid-electrolyte systems. Finally, perspectives on the design and synthesis

[1]State Key Laboratory of Biopharmaceutical Preparation and Delivery, Institute of Process Engineering, Chinese Academy of Sciences, Beijing 100190, China.
[2]School of Chemical Engineering, University of Chinese Academy of Sciences, Beijing 100049, China.
[3]School of Fashion and Textiles, The Hong Kong Polytechnic University, Hong Kong SAR, China.
[#]Authors contributed equally.

[*]**Correspondence to:** Dr. Jiangyan Wang, State Key Laboratory of Biopharmaceutical Preparation and Delivery, Institute of Process Engineering, Chinese Academy of Sciences, Beijing 100190, China; School of Chemical Engineering, University of Chinese Academy of Sciences, Beijing 100049, China. E-mail: jywang@ipe.ac.cn

strategies for phosphorus-carbon composites are provided in this mini-review.

INTRODUCTION

The need to increase energy supply and the exhaustion of non-renewable energy sources have led to the search for sustainable energy sources[1,2]. Although sustainable energy sources, including solar energy, wind energy, and hydro energy, have been widely discussed and implemented, their intermittent energy supply characteristics have led to the need to develop energy storage devices with high energy storage capacity. Lithium-ion batteries (LIBs) have emerged as one of the promising energy storage devices due to their high energy storage capacity, long lifespan, and low self-discharge characteristics. These characteristics have made LIBs one of the most promising energy storage devices for portable electronics, renewable energy storage systems, and electric vehicles (EVs)[3,4].

However, despite the success of LIBs, traditional anode materials, namely graphite, have almost reached their theoretical limits in terms of energy density. This has created a need to search for new materials to increase the power density and energy of LIBs. The biggest problem faced by traditional materials in this context has been their capacity and performance during fast charging[5]. The latest advancements in battery technology have been in the search for new anode materials to replace traditional materials and have been focusing on materials, for instance, silicon (Si)[6,7] and tin (Sn)[8] though they have their own disadvantages, specifically poor conductivity, high volumetric expansion, and poor cycling stability[9]. The search for anode materials for batteries, therefore, remains a critical issue[10].

Phosphorus (P) has been thoroughly investigated for Li storage in recent years[11,12]. While certain allotropes like black phosphorus (BP), are conductive, P-based anodes, particularly those based on RP, suffer from extremely low electronic conductivity and significant volume expansion during cycling (over 300%-500%), resulting in a limited cycle life for lithium storage applications[13]. Red phosphorus (RP) was the first P-based material to capture the interest of researchers due to its advantageous qualities as a potential anode material for LIBs, particularly due to its suitable insertion voltage and its high theoretical specific capacity of 2,600 mAh g^{-1}[14,15]. Although RP is readily obtained commercially, its low conductivity makes electrochemical reactions less reversible. In addition, the lithiated product Li_3P also shows poor performance, and the highly reactive surface of Li_3P may lead to significant electrolyte decomposition[16,17]. As an anode material, crystalline BP shows significantly better reversibility compared to RP.

To address these challenges, many efforts have been made over the last several years. The combination of phosphorus with carbon materials, i.e., mesoporous carbon[18], carbon nanotubes (CNTs)/nanorods[19], graphene[20,21] and graphite[22,23], not only improves the material's conductivity but also reduces the stress induced by volume variations during charge-discharge cycles. This review summarizes recent developments in the use of phosphorus-carbon composites as anodes for LIBs. It discusses the challenges and the lithium storage mechanism of phosphorus. Furthermore, it reviews the utilization of RP and BP-based materials in LIBs. Beyond conventional liquid-electrolyte systems, this review also examines the emerging applications of phosphorus-carbon anodes in all-solid-state batteries, highlighting the distinct failure mechanisms, including interfacial decomposition and contact loss, that arise from the use of solid electrolytes (SEs).

PHOSPHORUS-BASED ANODES FOR LIBs

Several allotropes of phosphorus exist: white phosphorus (WP), RP, and BP[24-26]. WP is highly reactive and toxic; thus, it is not suitable for use in batteries. RP and BP have gained increasing attention due to their stability [Figure 1A][27]. Amongst these materials, RP has been extensively studied due to its availability in the

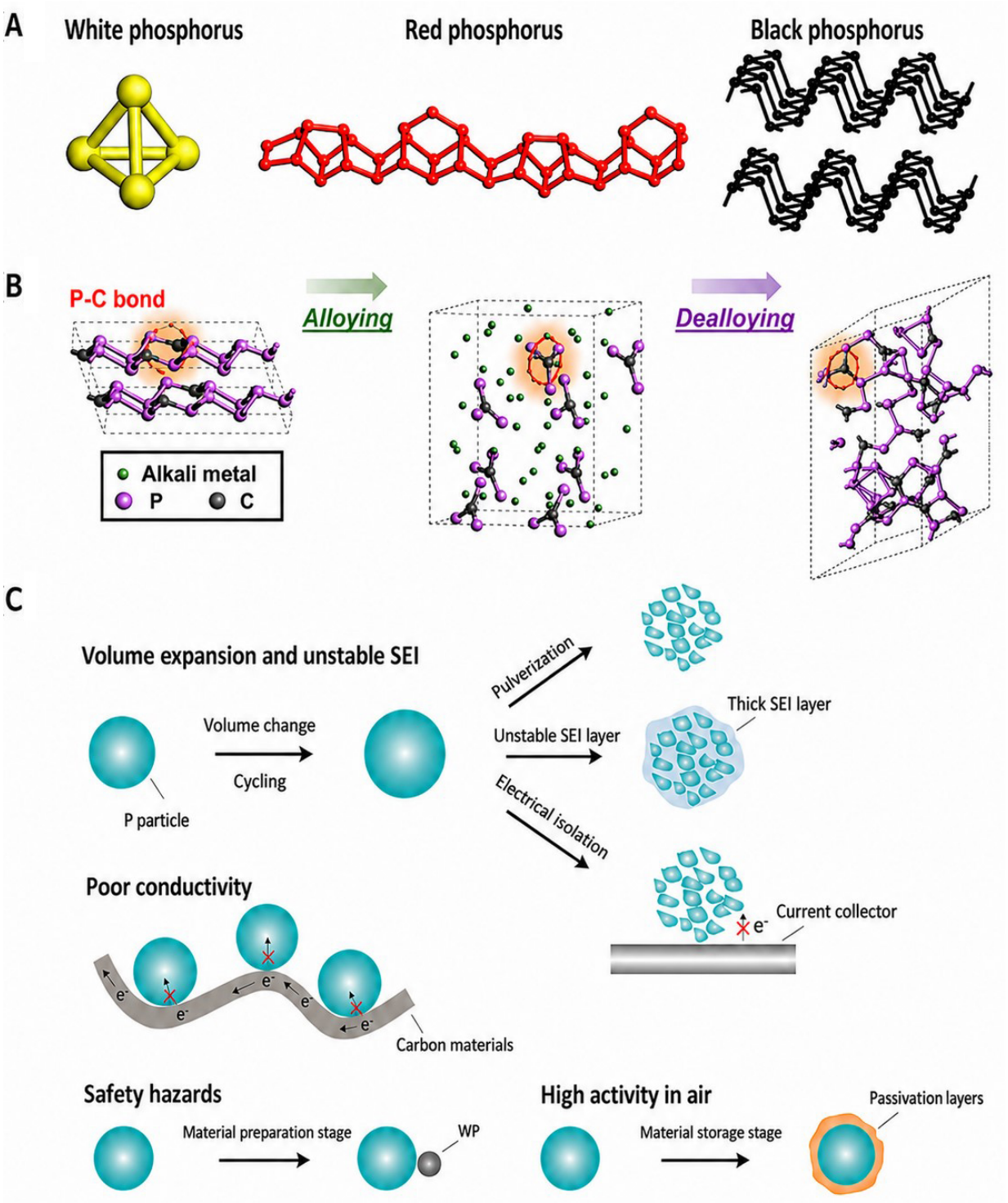

Figure 1. (A) Crystalline structures of WP, RP, and BP, adapted with permission from Ref.[27], copyright 2014, American Chemical Society; (B) Illustration of P-C bonds functioning as a recombination center for the regeneration of P-P bonds, adapted with permission from Ref.[30], copyright 2022, American Chemical Society; (C) Scientific challenges and technical issues for P anodes in AIBs, adapted with permission from Ref.[41], copyright 2020, Wiley.

market and ease of handling, but it has low conductivity and thus limited electrochemical activity. BP with high electrical conductivity has been found to have better activity than RP but still faces problems with conductivity and stability during cycling. To overcome these problems, it has to be integrated into a matrix to form an effective anode for LIBs[28,29].

Classification

Black phosphorus

BP is a two-dimensional semiconductor material with relatively high electrical conductivity (300 S m^{-1}). Similar to graphite crystals, BP has an orthorhombic crystal system and exhibits a black metallic luster[18]. Because of its extraordinarily high P-P bond binding energy[30,31] [Figure 1B], BP exhibits the lowest chemical reactivity and the highest density (2.70 g cm^{-3}) among all phosphorus allotropes. Since BP possesses a greater interlayer spacing (5.3 Å) than graphite (3.3 Å), ion intercalation occurs more easily[32]. Although BP is considered an attractive anode material for LIBs, its difficult and costly preparation hinders its practical application. Park *et al.*[33] synthesized BP and conducted the first systematic investigation of its lithium-storage capability through a high-energy mechanical milling process under ambient conditions. The transformation of the amorphous RP, which is obtained from commercial sources, into the orthorhombic BP structure yielded a composite material with superior electrochemical properties, which exhibited a stable capacity of 600 mAh g^{-1} after 100 cycles within the voltage window of 0.78-2.0 V, coupled with an enhanced initial coulombic efficiency (ICE).

Red phosphorus

RP has gained attention as a potential anode material owing to its high theoretical capacity of 2,596 mAh g^{-1}. This makes it an ideal material for high-performance LIBs[34]. However, RP is an electronic insulator, which necessitates the use of carbonaceous matrices to facilitate electron transfer[35]. A RP-carbon composite was synthesized by Sun *et al.*[36] using coconut shells that demonstrated competitive rate capability and cycle life by retaining 90% capacity over 500 cycles in specific laboratory conditions. In addition, phosphorus anodes generally suffer from poorer cycling stability than LTO or graphite due to significant volumetric expansion during lithiation, yet which could be improved by constructing a phosphorus-carbon composite. Wang *et al.*[37] used the evaporative condensation technique to coat hierarchical porous carbon nanofibers (HPCNFs) with RP. The P-HPCNFs anode showed high cycling stability after 100 cycles, with a reversible capacity of 883 mAh g^{-1}. The structural stability of the HPCNFs ensured the stability of the anode, and at the same time, the electrical conductivity was provided by the HPCNFs, and the electrochemical reaction interface and the volume changes were effectively addressed by the hierarchical porous structure. Cheng *et al.*[38] mixed both graphite and RP using an efficient ball milling method to produce nano RP/graphite composites. Consequently, P-C and P-O-C covalent bonds formed between graphite and RP. RP/G thus displays enhanced cyclic stability compared to RP. RP/G retains a specific capacity of 1,713 mAh g^{-1} even after 600 cycles at a current density of 1.30 A g^{-1}.

Challenges and limitations for phosphorus anodes

Although P-based anodes provide significant advantages for fast-charging LIBs, their actual application is constrained by a number of intrinsic and interfacial problems. These limitations stem from the fundamental structural, electrochemical, and transport characteristics of elemental P, particularly at high rates. A thorough grasp of these challenges is essential for the rational design of high-performance P-based anode materials.

Large volume expansion

During lithiation, P-based anodes can experience severe volumetric expansion (up to about 300%). The electrode architecture is subjected to significant mechanical strain as a result of this significant volume variation, which causes structural disruption and destabilization of the solid electrolyte interphase (SEI) layer. The SEI is essentially Li^+ conductive yet electrically insulating. Particularly during fast charging, the mechanical integrity and continuity of the SEI layers are essential for maintaining quick Li^+ transit and avoiding ongoing electrolyte breakdown. The dynamic fracturing and repair of the SEI layer during repeated

lithiation/delithiation have been demonstrated using operando electrochemical atomic force microscopy (EC-AFM) in conjunction with *ex-situ* spectroscopic investigations[39,40]. In addition to accelerating electrolyte breakdown, this ongoing rupture-reformation results in a steady loss of active P species and a gradual thickening of the interfacial layer, which eventually raises impedance, reduces rate capability, and shortens cycling life. Because there is no long-range structural support, the isotropic but significant expansion (~300%) in amorphous RP causes structural pulverization and sustained disintegration [Figure 1C][41]. The anisotropic lattice in BP causes directional expansion, which is much greater along the armchair direction than along the zigzag, causing interlayer slippage and local stress accumulation, which accelerate the development of fractures[42,43]. Because of its smaller dimensionality, monolayer or few-layer phosphorene shows improved mechanical compliance despite having the same lattice symmetry as BP. This increases the effectiveness of strain relaxation during lithiation, but the ultrathin nature also exposes a greater surface area to the electrolyte, making it vulnerable to interfacial instability and fracture if not appropriately protected[44].

Dissolution of lithium polyphosphide species

During the lithiation and delithiation processes of P-based anodes, several lithium polyphosphide compounds are created as metastable intermediates[13]. Furthermore, P-based electrodes can react with electrolyte components to produce unwanted compounds, thereby damaging their integrity[45]. Active P-containing moieties constantly dissolve and move away from the electrode because these species are soluble in conventional carbonate-based electrolytes. This process results in irreversible loss of active material and drastically lowers CE and reversible capacity over extended cycles. Additionally, the dissolved polyphosphide anions can diffuse across the electrolyte and perform redox reactions at the counter electrode, creating a shuttle effect similar to that observed in Li-S batteries. By promoting electrode corrosion and unregulated SEI growth, this parasitic behavior not only consumes cyclable lithium but also speeds up capacity fading and performance degradation[46].

Low electrical conductivity

Elemental P, particularly RP, suffers from extremely low electronic conductivity (~10^{-14} S cm^{-1}), which severely limits electron transfer and active material utilization. This poor conductivity leads to high charge-transfer resistance, sluggish reaction kinetics, and large polarization under high current densities, ultimately degrading rate capability and power performance[47,48].

Uncontrollable phosphorus oxidation

Despite being the thermodynamically most stable allotrope of phosphorus, the chemical adsorption of oxygen is made possible by the buckled layer structure and $3s^2$ $3p^3$ electron configuration of BP, which are favorable to the presence of lone pair electrons. As a consequence, BP is susceptible to irreversible oxidation with oxygen and water, which produces phosphorus oxides. This redox interaction between BP and oxygen creates oxidized defect sites along the edge plane of BP. O_2 chemisorption introduces hydrophilic dipolar species, which accelerate the degradation, particularly at the edge-site P atoms[49]. Similarly, RP oxidizes in air on its own. These oxidation processes ultimately result in the formation of several PO_x species on the phosphorus surface, which gradually yield hydrophilic intermediates exemplified by P_4O_6 and P_4O_{10}. These oxides fundamentally alter the electronic and material properties of phosphorus, impacting its performance in energy storage. By carefully controlling the oxidation of phosphorus anodes to produce a homogeneous surface layer, battery performance might be improved while stability and safety are maintained[50].

Mechanism of lithium-ion storage using phosphorus anodes

BP and RP exhibit distinct lithium-storage mechanisms. Lithium storage in BP is carried out by an intercalation mechanism in which Li^+ is inserted into the puckered layers through anisotropic diffusion along

zigzag channels (density functional theory (DFT)-calculated D_{Li^+}: 10^{-4} cm^2 s^{-1} in LiP_5) within the voltage window of 0.7-0.5 V without breaking P-P bonds and while maintaining structural integrity (≤ 4% volume change). BP can undergo destructive conversion to Li_3P during deep discharge at < 0.5 V, which irreversibly collapses its crystalline framework[51]. In contrast, amorphous RP lithiation follows a direct multistep alloying mechanism, progressing from P_4 tetrahedral to intermediate clusters Li_xP_y (LiP_7, LiP_5, Li_3P_7 at > 0.8 V) and finally forming crystalline Li_3P below 0.4 V. The $Li_{3+x}P$ phase forms due to excess lithiation[52]. RP suffers from poor kinetics but can be stabilized by carbon pore confinement, which buffers volume changes, while BP initially enables faster ion transport but requires covalent P-C bonding to prevent irreversible structural collapse during cycling.

APPLICATIONS OF PHOSPHORUS-CARBON COMPOSITE ANODES

0D materials

0D nanoscale architectures provide significant kinetic and mechanical benefits by reducing Li-ion diffusion lengths and relieving the internal stress accumulated during the lithiation and delithiation cycles. Crucially, the implementation of 0D domains serves to hinder crack propagation and delay the pulverization commonly observed in bulk phosphorus materials, particularly when the particles, represented by 4.5 nm quantum dots (QDs), are maintained below the critical threshold for strain-induced fracture[53]. Despite these structural advantages, 0D materials are inherently limited by their high surface energy, which creates a strong propensity for particles to collapse and aggregate during electrochemical applications. To mitigate these instabilities and prevent the loss of electrical contact, current research focuses on molecular-level dispersion within conductive matrices, specifically nitrogen-doped graphene, which acts as a secondary buffer to stabilize the 0D structure[54].

While dimension reduction addresses macroscopic strain, the fundamental durability of phosphorus is governed by atomistic phase transitions during lithiation[55]. Operando investigations reveal a complex layer-cage-chain-ion transition where lithiation initially targets the armchair P-P bonds, which are more susceptible to breakage than zigzag bonds due to their specific electronic states and longer bond lengths. As the lithium concentration reaches 50%, the framework evolves into P_7 cages (Li_3P_7), a structure uniquely favored by its minimal binding energy [Figure 2A][56]. However, deep lithiation to Li_3P causes irreversible structural amorphization, accompanied by a sharp density decrease from 2.022 to 1.47 g cm^{-3}. This volumetric collapse results in a catastrophic loss of electrical contact and capacity fade. Investigation into these phase evolution dynamics suggests that elevating the discharge cutoff voltage to 0.60 V can strategically avoid deep-discharge failure, increasing capacity retention to 80.2% by preserving the crystalline framework. The intrinsic performance is further supported by a low Li-ion diffusion barrier of 0.08 eV and a self-healing mechanism of the phosphorene framework at low lithium levels (< 25%). Understanding these fundamental atomic rearrangements provides a blueprint for managing the structural expansion that dictates the overall lifespan of phosphorus-based anodes, shifting the focus from simple particle size reduction to precise voltage and phase control[57].

To realize the potential of 0D phosphorus while overcoming aggregation, Pan *et al*.[58] developed van der Waals heterostructures featuring BP QDs distributed at a molecular level on nitrogen-doped (N-doped) graphene nanosheets. The electrochemical reaction mechanism follows a multi-step sequence of BP → Li_xP → Li_3P with distinct reduction peaks observed at 0.82, 0.61, and 0.01 V. The stability of this heterostructure arises from a size-stabilization effect where the 4.5 nm QDs remain below the critical threshold for strain-induced fracture, while the N-doped graphene matrix provides a dual-benefit: its 2D architecture buffers mechanical stress, and its pyridine-N groups create active regions that enhance interfacial interactions [Figure 2B]. This synergy significantly reduces charge-transfer resistance to 28.1 Ω, enabling the anode to deliver a high reversible capacity of 470 mAh g^{-1} at 5,000 mA g^{-1} [Figure 2C]. Critically, the molecular

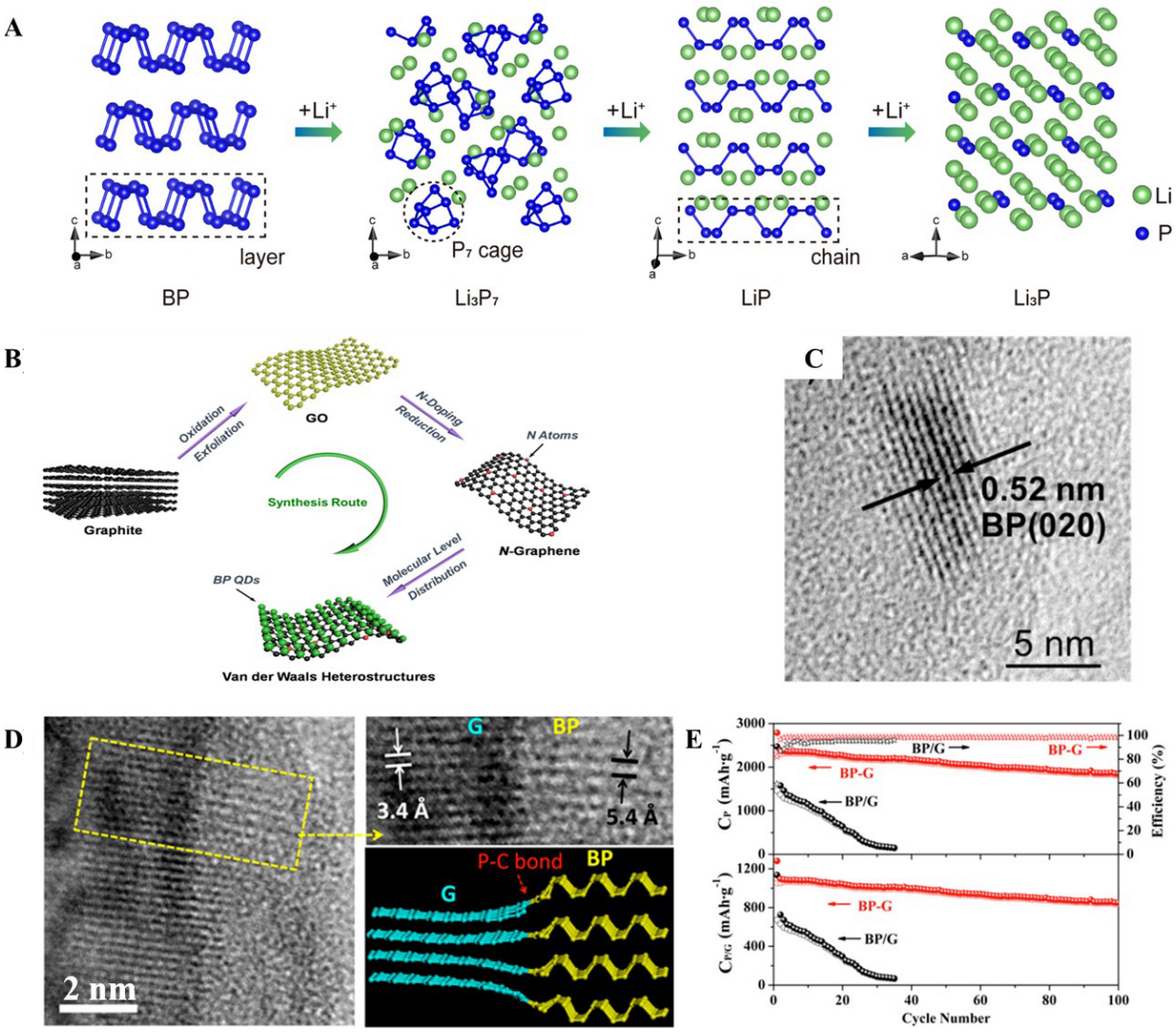

Figure 2. (A) Illustrations of layered BP, Li_3P_7 with P_7 cages, LiP with helical chains, and Li_3P with isolated P ions. Li and P atoms are shown by green and blue spheres, respectively, and the blue lines represent P-P bonds, adapted with permission from Ref.[56], copyright 2024, American Chemical Society; (B) Schematic illustration of the synthesis route for van der Waals heterostructures of BP QDs distributed on N-graphene nanosheets at the molecular level. (C) HRTEM image of BP QDs. (D) High-resolution TEM image alongside a schematic illustration of the BP-G composite. (E) The cycling behavior and Coulombic efficiency of BP/G and BP-G electrodes at 0.2 C. (B and C) are adapted with permission from Ref.[58], copyright 2016, Elsevier; (D and E) are adapted with permission from Ref.[27], copyright 2014, American Chemical Society.

dispersion facilitates the formation of a thicker and more stable SEI, which further mitigates capacity fading during long-term cycling. By integrating 0D QDs with a functionalized 2D host, the system effectively transforms inherently fragile phosphorus into a high-rate, stable energy storage medium suitable for high-power applications.

Building upon the need to manage volumetric expansion at the interface, Sun *et al.*[27] utilized high-energy mechanical milling to engineer chemically bonded black phosphorus-graphite (BP-G) composites [Figure 2D]. This mechanochemical approach facilitates the formation of robust P-C bonds, which serve as a stable mechanical backbone and persistent electrical pathway during cycling. This interfacial durability stems from π-p^* conjugation within sp^2 hybridized P-C bonds found at graphite edges and aromatic rings. These covalent linkages remain intact throughout electrochemical processes, preventing the pulverization and loss of electrical contact that typically plague physical mixtures [Figure 2E]. Consequently, the BP-G architecture

exhibits enhanced rate performance, maintaining a specific capacity of 1,240 mAh g^{-1} even at a high current density of 4.5 C. Electrochemical impedance spectroscopy confirms that this bonded structure significantly reduces charge-transfer resistance and enhances lithium-ion diffusivity compared to non-bonded counterparts. The synergy between covalent stabilization and improved kinetics allows for 80% capacity retention over 100 cycles, transforming BP from an unstable material into a viable candidate for high-power energy storage. This strategy demonstrates that tailoring the interfacial chemistry between the active material and the conductive host is essential for maintaining electrode integrity under severe mechanical strain while ensuring high phosphorus utilization through a stable conductive network.

Complementary to BP research, the stabilization of RP requires managing both massive expansion and the dissolution of lithium polyphosphide (Li_xPPs) intermediates. To address these challenges, a high-wrinkle carbon sphere (C_H) host was engineered using a vaporization-condensation strategy. Mechanistically, the curved topology of the C_H host provides a high binding energy for P_4 molecules, which accelerates their adsorption and subsequent polymerization into stable RP during synthesis. The electrochemical resilience of the RP-C_H composite is defined by robust P-C bonding and the strong adsorption of soluble intermediates, effectively suppressing the shuttle effect during cycling. This architecture ensures notable rate performance, with the RP-C_H composite delivering a capacity of approximately 600 mAh g^{-1} at current densities as high as 2,500 mA g^{-1}. Additionally, the RP-C_H configuration exhibits minimal polarization ΔE_p = 0.52 V, signifying significantly reduced charge-transfer resistance and enhanced lithium-ion transport kinetics compared to flatter carbon hosts[59]. By utilizing topological engineering to create a wrinkled conductive framework, this design successfully balances the requirement for mechanical buffering with the need for chemical sequestration of polyphosphide species. This approach highlights the importance of host morphology in optimizing the electrochemical resilience and kinetics of high-capacity phosphorus anodes, providing a scalable pathway for next-generation energy storage systems.

1D materials

One-dimensional (1D) nanomaterials, including CNTs and carbon nanofibers, are extensively utilized as frameworks for phosphorus anodes due to their ability to provide continuous percolation pathways for efficient electron transport. Their inherent mechanical flexibility allows these structures to accommodate the significant volume variations associated with phosphorus lithiation, thereby maintaining electrode integrity. Furthermore, 1D channels, particularly those in mesoporous carbon, offer shortened radial diffusion paths for ions and electrons, which are essential for high-rate operations[60]. However, a primary disadvantage of 1D hosts is the challenge of achieving high phosphorus mass loading. In CNT-based systems, loading is often limited to less than 50 wt% because phosphorus tends to coat the outer surfaces rather than infiltrate the internal cavities. This preference leads to the formation of thick, non-uniform layers that are susceptible to cracking and subsequent electrical disconnection during cycling. Additionally, while 1D materials facilitate longitudinal transport, ensuring stable interfacial contact between the active phosphorus and the conductive framework remains a critical hurdle, often requiring advanced chemical bonding or encapsulation strategies to prevent the mechanical pulverization and capacity decay typically observed in simpler physical mixtures[61].

Building on the structural advantages of 1D confinement, the integration of amorphous RP into the highly ordered mesoporous channels of CMK-3 effectively addresses the material's insulation and expansion issues. This architecture utilizes ~4 nm pores to restrict particle size and ensure high interfacial contact with the conductive matrix. The reaction mechanism involves a multi-stage electrochemical conversion ($3M + P \rightarrow M_3P$; M = Li, Na), achieving a reversible capacity of approximately 2,250 mAh g^{-1} at 0.25 C. A critical evaluation of this 1D confinement strategy reveals that even without covalent P-C bonding, the physical encapsulation within the CMK-3 backbone prevents mechanical pulverization and loss of electrical

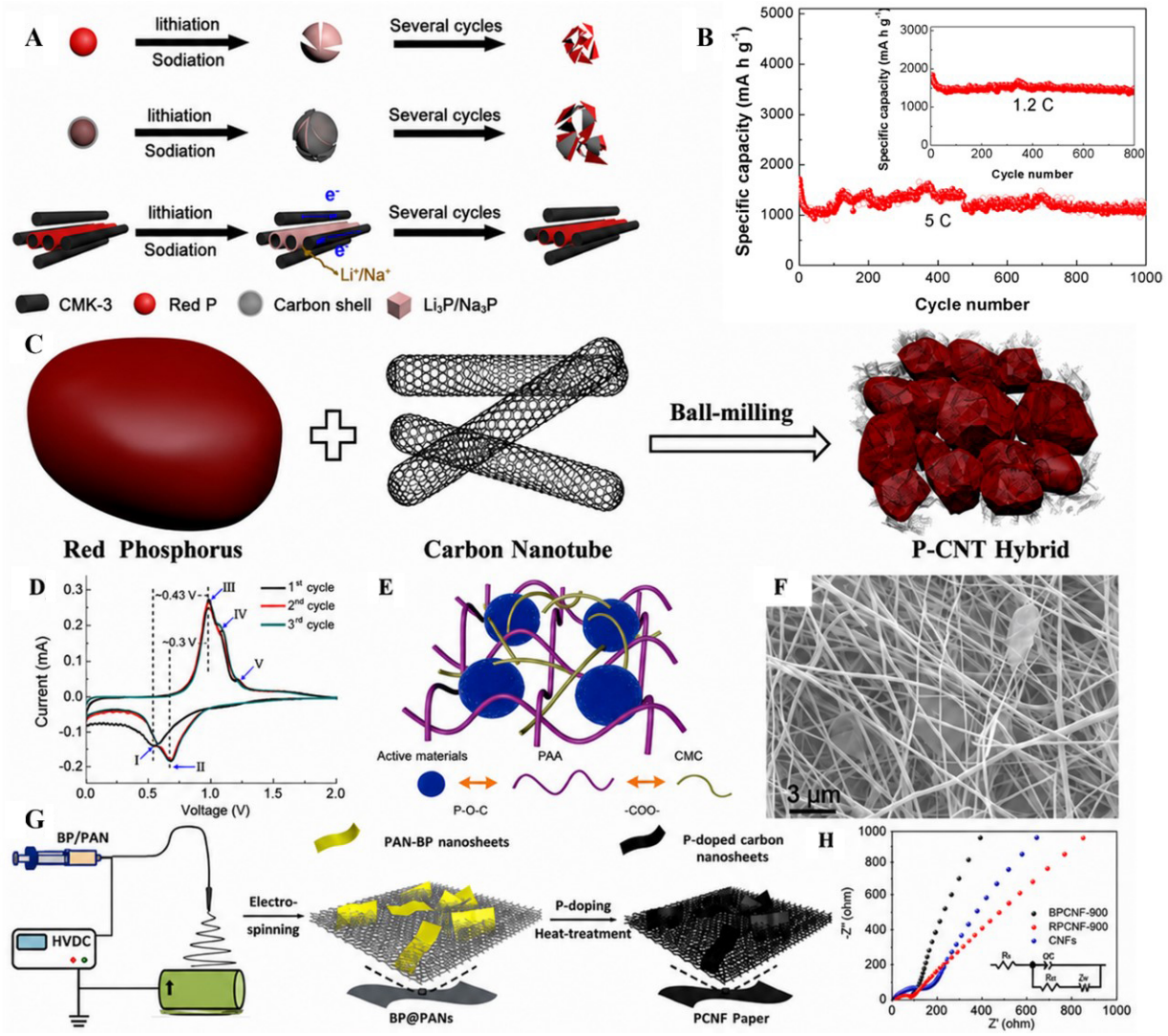

Figure 3. (A) Schematic illustration of the lithiation/sodiation process of RP particles, RP particles-carbon core-shell composite, and nanostructured RP confined in the channels of CMK-3 in LIBs and NIBs. (B) Stable cycle performance of P@CMK-3 electrodes for LIBs. (C) Schematic illustration of the synthesis of phosphorus-carbon nanotube (P-CNT) hybrid. (D) Cyclic voltammetry of the P-CNT hybrid anode measured between 0.01 and 2 V (*vs.* Li/Li$^+$) at a scan rate of 0.02 mV s^{-1}. (E) Schematic diagram of P/CNT-PAA/CMC. (F) SEM images of BPCNF. (G) Illustration of the preparation process of PCNF paper. (H) Nyquist plots and equivalent circuit models of BPCNF-900, RPCNF-900, and CNFs. (A and B) are adapted with permission from Ref.[62], copyright 2016, American Chemical Society; (C and D) are adapted with permission from Ref.[63], copyright 2019, Elsevier; (E) is adapted with permission from Ref.[64], copyright 2024, Wiley; (F-H) are adapted with permission from Ref.[65], copyright 2018, Elsevier.

connectivity. These 1D channels serve a dual function: they provide a stable mechanical framework to manage strain while facilitating rapid ion transport. Consequently, the composite demonstrates robust rate performance, delivering 1,598 mAh g^{-1} at 6.1 C for LIBs and maintaining 1,150 mAh g^{-1} over 1,000 cycles [Figure 3A]. This strategy illustrates that precise physical confinement within 1D channels can significantly enhance the durability and kinetics of phosphorus-based electrodes, even in the absence of chemical anchoring [Figure 3B][62].

Advancing interfacial engineering through mechanochemical synthesis, amorphous phosphorus-carbon nanotube (P-CNT) hybrids utilize covalent bridging to ensure structural integrity [Figure 3C]. High-energy ball-milling transforms bulk phosphorus into a nanoscale phase uniformly distributed throughout the CNT matrix, forming covalent P-O-C bridges. These bridges create a persistent electrical pathway that remains

intact during the multi-stage phase transitions predicted by DFT calculations ($Li_3P \rightarrow LiP \rightarrow Li_3P_7 \rightarrow LiP_7 \rightarrow P$ during delithiation)[63]. The structural integrity of the P-CNT hybrid is defined by this chemically bonded interface, which prevents the active material from losing electrical contact despite massive mechanical strain. Critically, the reduction in particle size to the submicron level decreases cell polarization and enhances the kinetics of the electrochemical conversion. This architecture exhibits a rate capability of 1,081 mAh g^{-1} even at an extreme current density of 3,900 mA g^{-1} [Figure 3D]. Upon returning to lower rates, the capacity recovers significantly, illustrating the high reversibility and resilience of the amorphous bonded structure. This method represents a scalable strategy for mitigating the intrinsic electrical and mechanical limitations of elemental phosphorus through atomic-level interfacial control.

To further reinforce the stability of 1D frameworks, the development of a 3D cross-linked PAA/CMC binder system offers a chemical approach to managing volume expansion. This binary system undergoes thermal condensation to facilitate esterification, creating a rigid mechanical network that establishes stable P-O-C chemical bonds with the phosphorus surface [Figure 3E]. This robust anchoring significantly bolsters the mechanical strength of the electrode and ensures a high affinity for phosphorus, evidenced by a low contact angle of 22.4. Assessment of this polymeric anchoring shows that the PAA/CMC framework restricts the expansion of the P/CNT composite to a mere 6%, a stark improvement over the 83% observed with traditional PVDF binders. Mechanistically, the binder does not react with Li_3P intermediates, which preserves its viscosity and reduces irreversible capacity loss. These improvements lead to significantly reduced charge-transfer resistance and enhanced lithium-ion diffusion kinetics. The resulting rate performance is remarkable, with the anode delivering a specific discharge capacity of 1,215.3 mAh g^{-1} at a high current density of 5,200 mA g^{-1}. This approach demonstrates that engineering the binder interface is as critical as the conductive host for transforming unstable phosphorus into a high-performance, fast-charging material[64].

Complementing composite strategies, the immobilization of heteroatoms within 1D carbonaceous frameworks provides a bottom-up solution for tailoring electrode properties. By using BP as a doping source, phosphorus-doped carbon nanosheets and nanofibers are synthesized with a high doping level of 3.7 wt%. The reaction mechanism centers on the uniform distribution of phosphorus via intrinsic P-C and P-O covalent bonding, which enhances both electronic conductivity and electrochemical reactivity [Figure 3F]. This structural-performance synergy is optimized by the interwoven 1D configuration, which provides an interconnected network of rapid transport pathways while accommodating mechanical strain. Unlike surface-loaded composites, phosphorus is integrated into the carbon lattice, ensuring long-term durability [Figure 3G]. The resulting composite exhibits extraordinary rate performance, delivering a reversible capacity of 200 mAh g^{-1} at a current density as high as 20,000 mA g^{-1}. Furthermore, it maintains 607 mAh g^{-1} after 700 cycles at 1,000 mA g^{-1} [Figure 3H]. This research highlights that atomic-level doping within 1D frameworks can achieve extreme rate capabilities and sustained stability, offering a viable path for high-power, free-standing anodes that do not require additional binders[65].

Finally, to address the challenges of interfacial instability and intermediate dissolution, a core-shell BP/CNT@PPy architecture has been engineered. This design features an internal CNT network for conductivity and an external flexible polypyrrole (PPy) shell that acts as an elastic mechanical buffer and protective barrier. XPS analysis confirms the formation of covalent P-C bonds between the BP and CNTs, ensuring electrical contact during cycling. The electrochemical process is characterized by highly reversible delithiation peaks at 1.24 and 1.32 V, while the PPy coating effectively mitigates the polyphosphide shuttle effect. DFT calculations indicate that PPy provides strong binding energies (1.09 to 1.91 eV) to chemically adsorb soluble phosphorus intermediates, confining them within the electrode[66]. Although the lithiation-inactive shell initially results in a slightly lower discharge capacity, this core-shell configuration achieves a

reversible capacity of 1,376.3 mAh g^{-1} after 200 cycles at 260 mA g^{-1}. This core-shell strategy demonstrates that combining covalent bonding with polymer encapsulation can transform unstable high-capacity materials into resilient energy storage components by simultaneously managing mechanical strain and chemical intermediate dissolution.

2D materials

The integration of graphene with BP offers robust mechanical properties due to its larger specific surface area and higher electrical conductivity, thereby mitigating volume variations and improving the long-term cyclic stability[67]. However, in spite of these unique features, some disadvantages of graphene have been identified. One of the disadvantages is the low density of the graphene sheets, which affects their capacity. Also, the re-stacking of the graphene sheets results in the loss of their unique properties. In addition, the synthesis of graphene with a large surface area and highly conductive graphene is complex, and controlling the development of impurities/defects on graphene sheets is exceedingly tough[68].

First-principles calculations on lateral heterostructures (BP-G) provide deeper insights into how covalent interfacial engineering resolves the detrimental edge reconstruction common in phosphorene nanosheets. The stabilization mechanism involves phosphorus and carbon atoms forming sp^2-hybridized covalent bonds that saturate dangling bonds at the BP boundaries. This structural modification effectively improves electronic conductivity by shifting the Fermi level, transforming the semiconducting phosphorene into a metallic hybrid system. Analysis of the transport kinetics reveals that these P-C linkages reduce the Li-ion migration barrier at the interface to a mere 0.074 eV, compared to the 0.52 eV barrier found in reconstructed edges[69]. This facilitates rapid lithium transport along the zigzag direction with an overall low barrier of approximately 0.12 eV. The rate performance derived from these optimized kinetics is reflected in a theoretical specific capacity of 426.92 mAh g^{-1}, outperforming commercial graphite. Critically, the lateral integration prevents the sharp increase in resistance typically observed at nanosheet boundaries, ensuring that the high theoretical mobility of phosphorene is preserved in the composite. This atomic-level synergy confirms that covalent passivation is essential for both mechanical buffering and the optimization of charge-transfer kinetics in high-rate phosphorus anodes.

Building upon these composite strategies, Liu *et al*.[70] prepared a sandwich-structure thin-film anode by encapsulating a chemically bonded black phosphorus-graphene hybrid (BPGO) between stacks of graphene. The internal reaction mechanism centers on the formation of covalent P-C and P-O-C bonds during a mild solvothermal process, which anchors BP to the reduced graphene oxide (RGO) sheets [Figure 4A]. These robust chemical linkages serve as a stable backbone, protecting the BP nanosheets from cracking during the severe mechanical strain of lithium intercalation. A notable structural innovation is the replacement of traditional copper foil with graphene stacks, which function as both a flexible current collector and a protective barrier against electrolyte exposure. This binder-free architecture significantly enhances electrochemical kinetics, with the anode delivering a high specific capacity of 1,401 mAh g^{-1} even after 200 cycles at 100 mA g^{-1}. The rate performance is equally resilient; the composite maintains a capacity of approximately 656 mAh g^{-1} at a current density of 1 A g^{-1} and recovers nearly all its capacity when returned to lower rates, illustrating the stability of the chemically bonded interface. This design effectively resolves the low ICE and thermal instability of BP, transforming it into a commercially viable candidate for high-power, lightweight energy storage applications.

To realize the benefits of such 2D frameworks, a simplified solution-based assembly method has been developed to anchor amorphous nanoscale RP sheets onto highly conductive graphene layers. Mechanistically, this approach utilizes the opposite zeta potentials of RP and graphene in a mixed solvent to facilitate a stable hybrid structure in which P is uniformly loaded onto unfolded graphene sheets. The

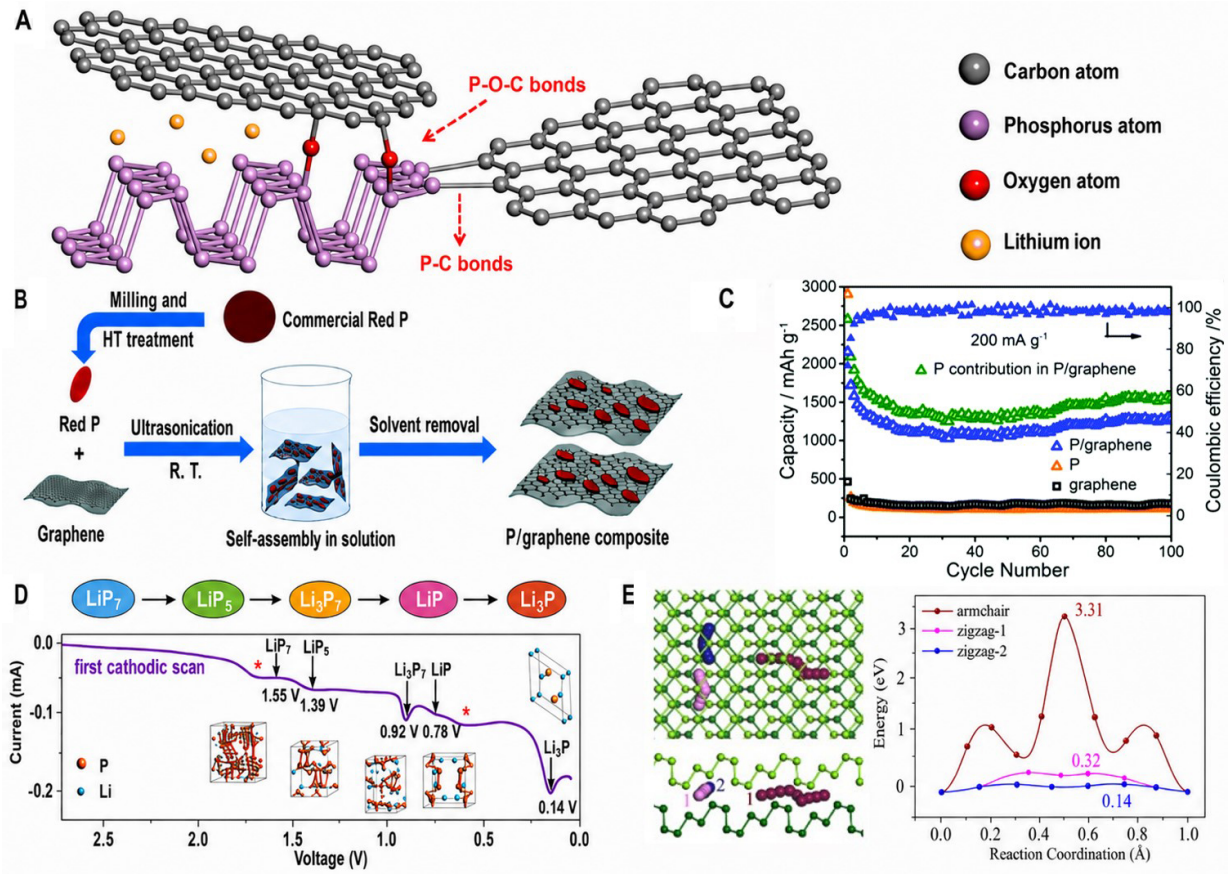

Figure 4. (A) Schematic of P-C bonds and P-O-C bonds in solvothermal BPGO and storage of Li^+, adapted with permission from Ref.[70], copyright 2017, Wiley; (B) The synthetic scheme of the P/graphene composite. (C) Cycling behavior of RP, graphene, and the P/graphene nanohybrid. (B and C) are adapted with permission from Ref.[71], copyright 2017, The Royal Society of Chemistry; (D) Schematic diagram showing five key states of the BP QD/TNS anode during the first CV cathodic scan, corresponding to different crystalline phases (LiP_7, LiP_5, Li_3P_7, LiP, and Li_3P) at specific discharge voltages, adapted with permission from Ref.[72], copyright 2018, Wiley; (E) Top view and side view of Li diffusion pathways and the corresponding energy profiles in bulk GP, adapted with permission from Ref.[73], copyright 2022, American Chemical Society.

synergistic interaction between the amorphous RP sheets and graphene layers distributes and relieves local mechanical strain to alleviate pulverization that typically causes electrode failure [Figure 4B]. Graphene acts as a porous, flexible buffer that accommodates volume variations and maintains a robust conductive network for efficient electron transfer. This configuration exhibits significant rate performance, delivering a high reversible capacity of 1,125 mAh g^{-1} at a current density of 1,000 mA g^{-1}. Evaluation of this design confirms that the solution-based strategy is safer and more energy-efficient than traditional vaporization-condensation methods, as it avoids the formation of toxic WP while preventing graphene restacking [Figure 4C]. Consequently, the composite maintains an intimate electrical contact through P-C surface interactions, significantly reducing charge-transfer resistance compared to pure phosphorus electrodes. This synergy between the flexible carbon host and the amorphous active material ensures high phosphorus utilization and structural integrity throughout repeated lithiation/delithiation cycles[71].

Further advancing the potential of BP, a dual-model energy storage (DMES) mechanism has been established by anchoring BP QDs onto Ti_3C_2 MXene nanosheets. This architecture facilitates a synergistic reaction mechanism where the BPQDs serve as a high-capacity alloying component, while the MXene provides rapid pseudocapacitive charge storage [Figure 4D]. The merits of this MXene hybrid are defined by strong P-O-Ti covalent bonds, which induce atomic charge polarization and enhance the binding affinity of the composite

for Li^+ ions. This polarization allows the composite to deliver reversible capacities that can surpass the theoretical alloying capacity of the components alone. In terms of rate performance, the BP QD/TNS composite displays high durability, maintaining a capacity of 520 mAh g^{-1} at a high current density of 1,000 mA g^{-1} after 2,400 cycles, with capacity retention over 100% due to the gradual activation of the active material. Evaluation of this hybrid system indicates that the low dimension of the BP QDs effectively shortens diffusion lengths and relieves mechanical stress, while the metallic conductivity of the Ti_3C_2 nanosheets ensures efficient charge transfer. By combining the high capacity of quantum-confined phosphorus with the fast kinetics of polarized MXene interfaces, this dual-mode strategy represents the most effective method for stabilizing phosphorus-based anodes for long-life battery systems[72].

Green phosphorus (GP) represents an emerging 2D anode material for LIBs, characterized by structural stability between black and blue phosphorus. Analysis reveals that GP surpasses BP in intercalation capacity; bulk GP achieves 288.4 mAh g^{-1} compared to 164.4 mAh g^{-1} for BP[73]. Furthermore, single-layer GP provides 432.7 mAh g^{-1}, showcasing the benefits of dimensionality reduction. Its kinetics are characterized by an ultrafast diffusion barrier of 0.14 eV along the zigzag direction, though extreme anisotropy limits armchair transport. Lithiation triggers a semiconductor-to-conductor transition via s-p hybridization, significantly improving electronic conductivity [Figure 4E]. While GP offers promising lithiation voltages (1.33-2.07 V) and high theoretical capacities (up to 2,596 mAh g^{-1}), realizing its potential requires overcoming hurdles in large-scale production and long-term structural stability during extended cycling. First-principles measurements show that the storage of lithium in GP is highly dependent on the number of layers, where the single-layer GP has a higher theoretical capacity than the other configurations, including the double-layer and bulk configurations, while maintaining structural stability. The lithium diffusion in the GP structure is also highly anisotropic, where the migration barrier in the zigzag direction is found to be low (~0.14 eV), thus showing favorable kinetic properties for fast charging of the batteries.

3D materials

While low-dimensional designs can effectively improve reaction kinetics and shorten ion-transport pathways, their limited structural tolerance under large and repeated volume variations can still restrict long-term durability. In this regard, three-dimensional (3D) hollow and porous architectures provide an attractive alternative because they integrate interconnected transport networks with internal free space for structural regulation[74,75]. The presence of interior voids and a porous skeleton reduces stress accumulation during charge/discharge cycling. Meanwhile, the open pore network improves electrolyte infiltration and increases the accessible electrode/electrolyte interface, which promotes uniform reaction distribution[76]. However, pore structure optimization remains challenging; if pores are too large (> 5 nm), phosphorus agglomerates and fails to maintain nanoscale confinement, while pores that are too small (< 1 nm) limit phosphorus loading and electrolyte infiltration[77,78].

The development of the Hoya-like triple-shelled architecture represents a significant advancement in phosphorus immobilization, utilizing a nitrogen-doped hollow MXene sphere (NM) integrated with a dual-sided porous carbon network (DCNM). The reaction mechanism involves a multi-stage electrochemical process where RP undergoes stepwise lithiation to Li_xP (x = 1-3), as indicated by cathodic peaks at 0.2 and 0.5 V [Figure 5A]. This architectural synergy, featuring a highly conductive NM wall and a micromesoporous carbon network, is critical for facilitating rapid electron transport while simultaneously providing the void space necessary to accommodate RP and buffer mechanical strain. According to Figure 5B, a critical evaluation of this configuration highlights the role of nitrogen heteroatoms in providing strong chemical adsorption for polyphosphide intermediates (binding energy of 11.46 eV for LiP_5)[79], which effectively suppresses the shuttle-like dissolution common in phosphorus electrodes. This architecture enables exceptional rate performance, delivering reversible capacities of 1,666.7 and 845.0 mAh g^{-1} at current

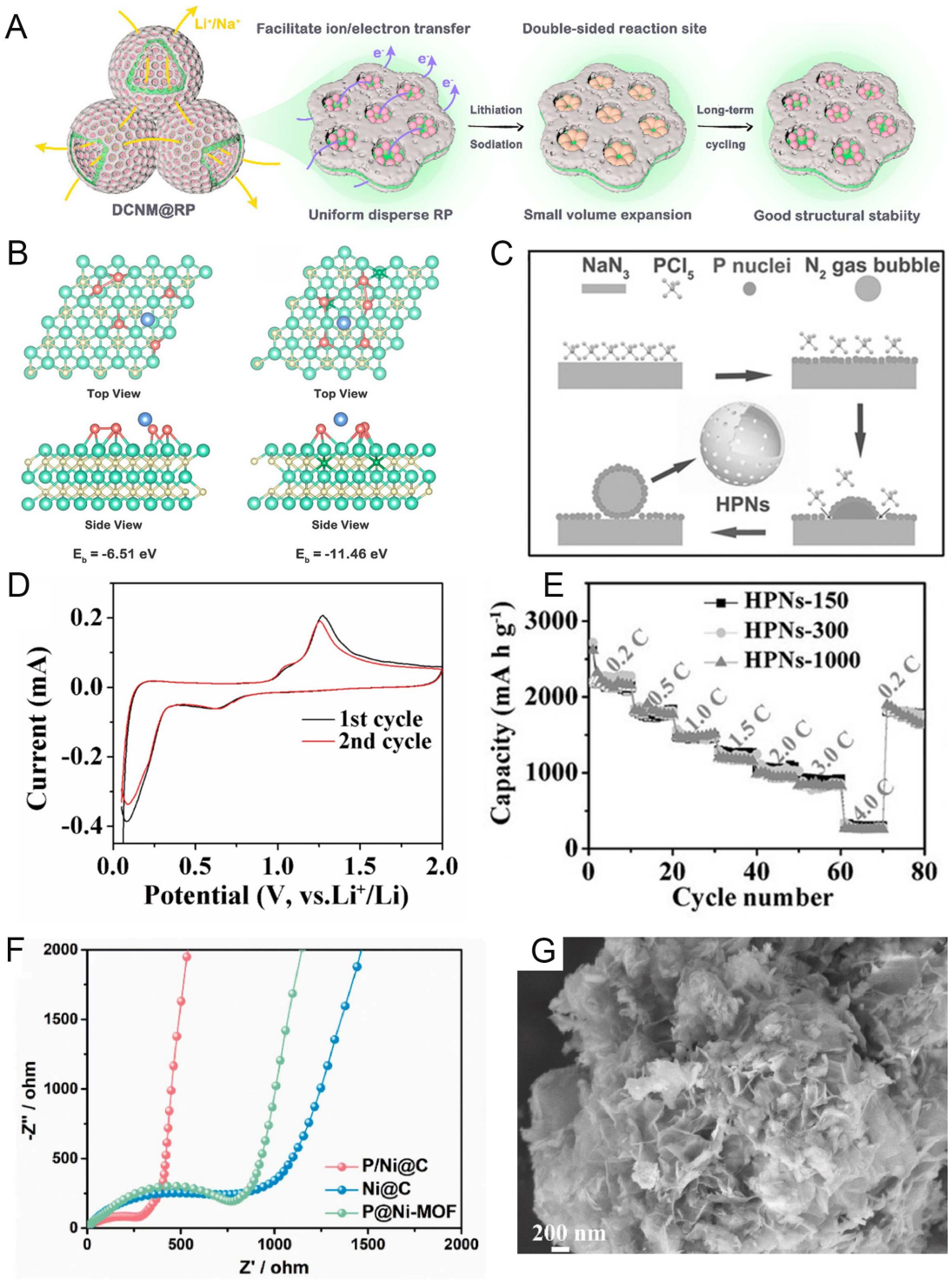

Figure 5. (A) Schematic illustration of the lithiation/sodiation and subsequent delithiation/desodiation processes of RP confined in the pores of DCNM in LIBs and SIBs. (B) Optimized structures and adsorption energies of LiP_5 on the Ti_3C_2 and N-doped Ti_3C_2 surfaces. Here, blue, red, yellow, light green, and dark green spheres represent lithium, phosphorus, carbon, titanium, and nitrogen atoms, respectively. (C) The schematics illustrate the proposed formation mechanism of the hollow phosphorous nanospheres. (D) The CV curves of HPNs-300 for LIBs anode with a scan rate of 0.1 mV s^{-1}. (E) The rate performance of HPNs with average diameters of 150 (HPN-150), 300 (HPNs-300), and 1,000 nm (HPNs-1000) for LIBs at current densities varying from 0.2 to 10.0 C. (F) Cycling performances of the P@Ni-MOF, P/Ni@C, and Ni@C electrodes. (G) SEM image of P/Ni@C composite. (A and B) are adapted with permission from Ref.[79], copyright 2023, American Chemical Society; (C-E) are adapted with permission from Ref.[80], copyright 2017, Wiley; (F and G) are adapted with permission from Ref.[81], copyright 2022, Elsevier.

densities of 2 C and 10 C, respectively. Furthermore, the DCNM@RP anode maintains a capacity of 1,360.7 mAh g^{-1} over 1,800 cycles at 2 C for lithium storage, demonstrating that the combination of physical

confinement and N-enhanced chemisorption creates a durable, high-rate electrochemical interface.

Advancing beyond traditional host-guest composites, the first wet-chemical synthesis of hollow RP nanospheres (HPNs) with porous shells offers a unique structural solution to pulverization. This solvothermal approach utilizes a gas-bubble-directed formation mechanism where N_2 gas acts as a template to generate uniform amorphous nanospheres with a diameter of ~300 nm and a shell thickness of ~40 nm [Figure 5C]. The mechanical resilience of these nanospheres centers on the porous hollow geometry, which provides sufficient interior void space to accommodate strain while the shell's porous channels facilitate efficient Li-ion/Na-ion migration. Unlike vaporization-condensation methods that often struggle with low mass loading, this wet-chemical route achieves a high phosphorus content of 60 wt%, which is critical for practical energy density. The electrochemical conversion proceeds to a fully lithiated Li_3P phase, supported by a remarkably low Warburg coefficient of 16.13 $\Omega\ S^{-1/2}$, signifying high ion diffusion kinetics. This structural resilience translates into unprecedented rate capability, with the HPNs maintaining a reversible capacity of 317.2 mAh g^{-1} at a super-high current density of 10 C. Long-term stability is evidenced by a capacity retention of 1,048.4 mAh g^{-1} after 600 cycles at 1.0 C, confirming that hollow amorphous structures can effectively maintain electrical contact without mechanical fracture [Figure 5D and E][80].

Metal-organic frameworks (MOFs) are a class of coordinated polymers characterized by their 3D porous architectures. Typically constructed from metal ion nodes interconnected by organic ligands, MOFs form extended crystalline networks with high surface areas and tunable porosity. However, recent studies on metal phosphide composites note that while porous carbon buffers volume expansion[77], it introduces additional inactive components that reduce overall energy density.

Refining the morphology of carbon hosts, the use of MOF-derived microflower-like carbon provides a highly tailored environment for phosphorus decoration. In this system, RP is anchored to a nickel MOF-derived matrix via a two-step solvothermal and heat treatment process, resulting in a P/Ni@C composite characterized by stable P-O-C covalent bonds. The reaction mechanism is enhanced by the presence of metallic nickel, which improves electronic transport and mechanical ductility, while the microflower structure provides numerous lamellar sheets to encapsulate phosphorus sites. This interfacial stabilization is primarily governed by stable covalent linkages that prevent the aggregation of active material and ensure persistent electrical pathways throughout cycling. Analysis of the charge-transfer resistance reveals that the P/Ni@C anode possesses a much lower value (172.9 Ω) compared to non-bonded counterparts, directly benefiting from the synergistic effect of the carbon framework and covalent anchoring [Figure 5F and G]. This architecture sustains a reversible capacity of 1,184.6 mAh g^{-1} over 400 cycles at 200 mA g^{-1}, illustrating that MOF-derived templates can be engineered to solve the poor interface compatibility and low capacity associated with traditional graphitic carbon[81].

Sustainable materials engineering further expands these capabilities through the use of biomass-derived N-doped hierarchically porous carbon (BDPC). Using tobacco stems as a precursor, a high-surface-area host (2,809 $m^2\ g^{-1}$) is synthesized to encapsulate nanoscale RP via a vaporization-condensation strategy. The reaction mechanism involves the infiltration of gaseous phosphorus into 1.2 nm micropores, where it is immobilized through N-doping and the formation of P-C and P-O chemical bonds. The efficiency of this biomass-derived anode is optimized by the hierarchical pore distribution; while micropores anchor the phosphorus, mesopores facilitate rapid electrolyte penetration and ion transport. A critical evaluation of the P@BDPC composite (62.1 wt% P) shows that it achieves a high ICE of 91.7%, as the internal deposition of phosphorus reduces direct electrolyte contact and subsequent side reactions. The rate performance is highly efficient, with the anode delivering 1,689 mAh g^{-1} at 500 mA g^{-1} and maintaining 599 mAh g^{-1} even at an extreme current density of 30 A g^{-1}. This stability is rooted in the carbon matrix's ability to buffer large

mechanical variations, allowing for 90% capacity retention over 600 cycles at 5 A g^{-1}[82]. This approach demonstrates that agricultural waste can be converted into high-performance, low-cost anodes by leveraging intrinsic heteroatom doping and complex pore architectures.

IN-SITU CHARACTERIZATION OF PHOSPHORUS-CARBON INTERFACES

In-situ characterization techniques allow for the real-time monitoring of morphological, compositional, and microstructural evolution during electrochemical cycling[83]. Significant changes in the electrochemical parameters, especially the cyclic stability of the electrodes, specific capacity of the electrodes for energy storage, and rate performance of the electrodes in the composite carbon-based anodes with different composite architectures are observed. The relationship between composite materials and energy storage performance must be understood, and the best and most advanced carbon-based composite anodes for LIBs must be developed.

In-situ Raman spectroscopy

Using the *in-situ* Raman method, Zhao *et al.*[61] investigated phosphorus in CNTs. The authors quantitatively linked the strain caused by the volume expansion of phosphorus to the structural integrity of the carbon host by tracking the shift in the G-band position in the carbon nanotubes in real time during the lithiation and delithiation processes. During the lithiation process, the G-band position in the P@DWCNT structure was shifted by up to 17 cm^{-1}, corresponding to a maximum tensile strain in the walls of the DWCNTs of up to 24 GPa. However, the G-band position was fully restored to its original position at 1,590 cm^{-1} upon delithiation, revealing the full relaxation of the strain and confirming the high reversibility of the P-DWCNT composite. This reversible behavior was attributed to the partial filling rather than complete filling of phosphorus within the DWCNTs, which allows the volume expansion to be accommodated along the nanotube axis. In contrast, P@SWCNT showed limited reversibility due to the fragile single-carbon layer, while P@MWCNT exhibited fast capacity degradation owing to excessive external phosphorus deposition that detached during cycling [Figure 6A-D].

In-situ TEM

The dynamic monitoring of volume expansion phenomena resulting from phase changes during the course of the material's energy storage process and significant volume changes resulting in crushing and deterioration of electrode material can be achieved via *in-situ* TEM. Kühne *et al.*[84] studied the reversible embedding of Li-ions in bilayer graphene using low-pressure *in-situ* TEM. The Li-ions were observed to diffuse and disperse rapidly and evenly between the graphene layers. Moreover, rather than storing the Li-ions at the edge of the graphene, they might be able to form a multi-layer structure in the bilayer graphene sheet in a stable and dense ordered manner [Figure 7A and B], thus enabling the Li-ions to be stored in the graphene at an extremely high capacity.

The electrochemical lithiation behavior of BP has been observed via *in-situ* TEM by Xia *et al.*[85] In the case of BP as an anode material, significant anisotropic size changes and phase changes were observed for a square BP material transforming into an amorphous Li_xP_y material during the course of lithiation. Moreover, during discharge, the BP anode material was abruptly ground into small pieces, resulting in poor cycling performance [Figure 7C-F].

In-situ X-ray diffraction and *in-situ* X-ray absorption spectroscopy

During the electrochemical cycling process, *in-situ* XRD can provide additional real-time information on the evolution of the electronic structure and phase transformation in the phosphorus-carbon anode[86]. The complete lithiation/delithiation mechanism of the BP-graphite-CNTs composite anode was investigated by Li *et al.*[87] using operando techniques as presented in [Figure 8A and B]. The new peaks corresponding to the

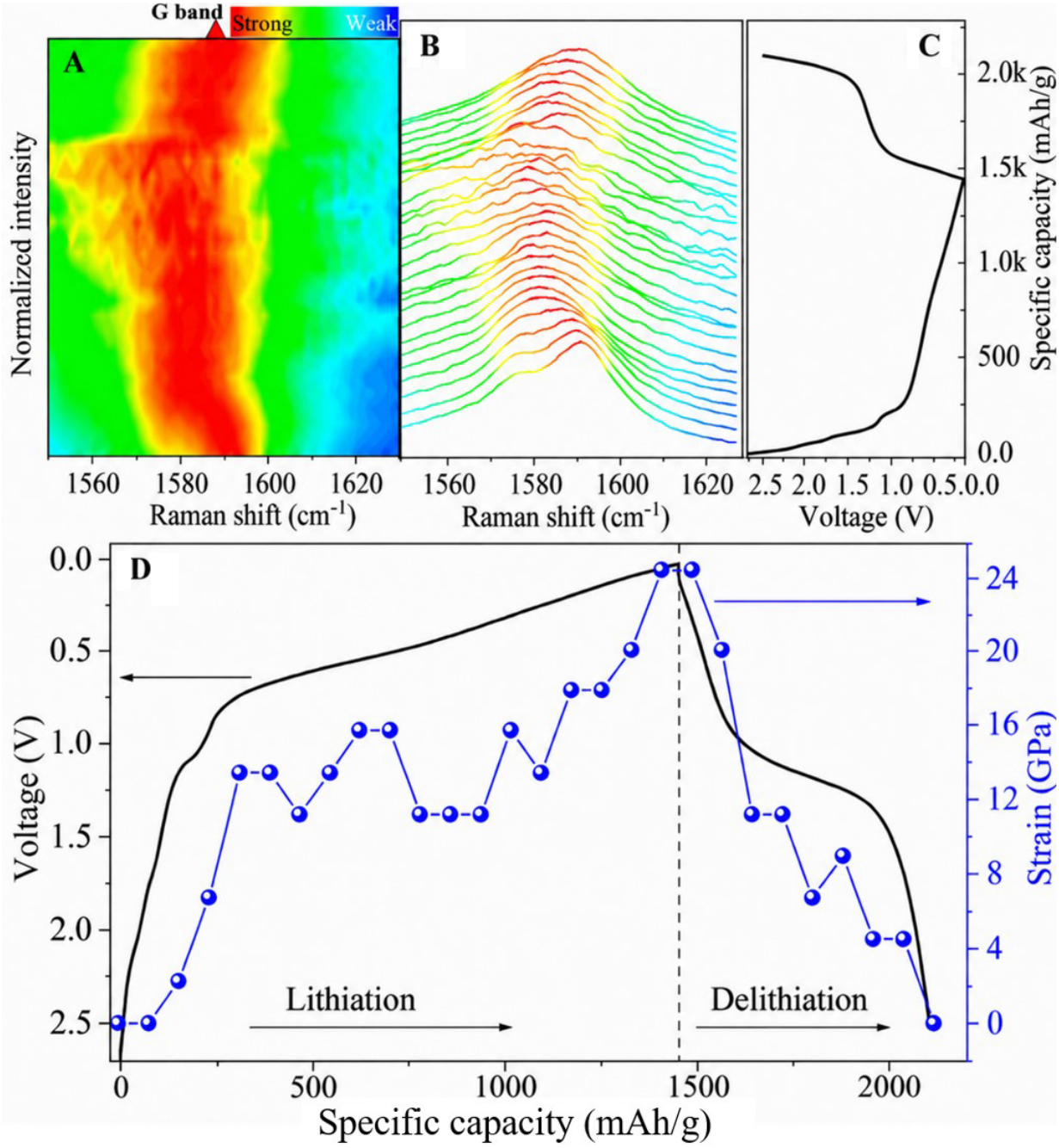

Figure 6. *In situ* Raman analysis of P@DWCNT during the galvanostatic lithiation/delithiation process. (A) Contour plot, (B) line plot, (C) corresponding lithiation/delithiation curve, and (D) G-band shifts and corresponding stress of P@DWCNT anode. The figure is adapted with permission from Ref.[61], copyright 2024, American Chemical Society.

crystalline Li_3P_7 phase emerge, and the intensity of the peaks corresponding to the BP phase decreases gradually and disappears at 1.206 V. The BP and Li_3P_7 phases coexist in the range of 1.206 to 0.893 V. The Li_3P phase peaks emerge at 0.799 V. The peaks corresponding to the Li_3P_7 phase decrease. The XRD peaks corresponding to the intermediate LiP phase were not detected because they were in the amorphous state. The P K-edge absorption edge was found to gradually shift to lower energy with discharge, indicating the gradual filling of the P 3p orbitals with electrons provided by lithium, according to the operando XAS results [as shown in Figure 8C and D], which supported this by investigating the local electronic structure. Five different chemical states were identified by five different spectral characteristics during various discharge

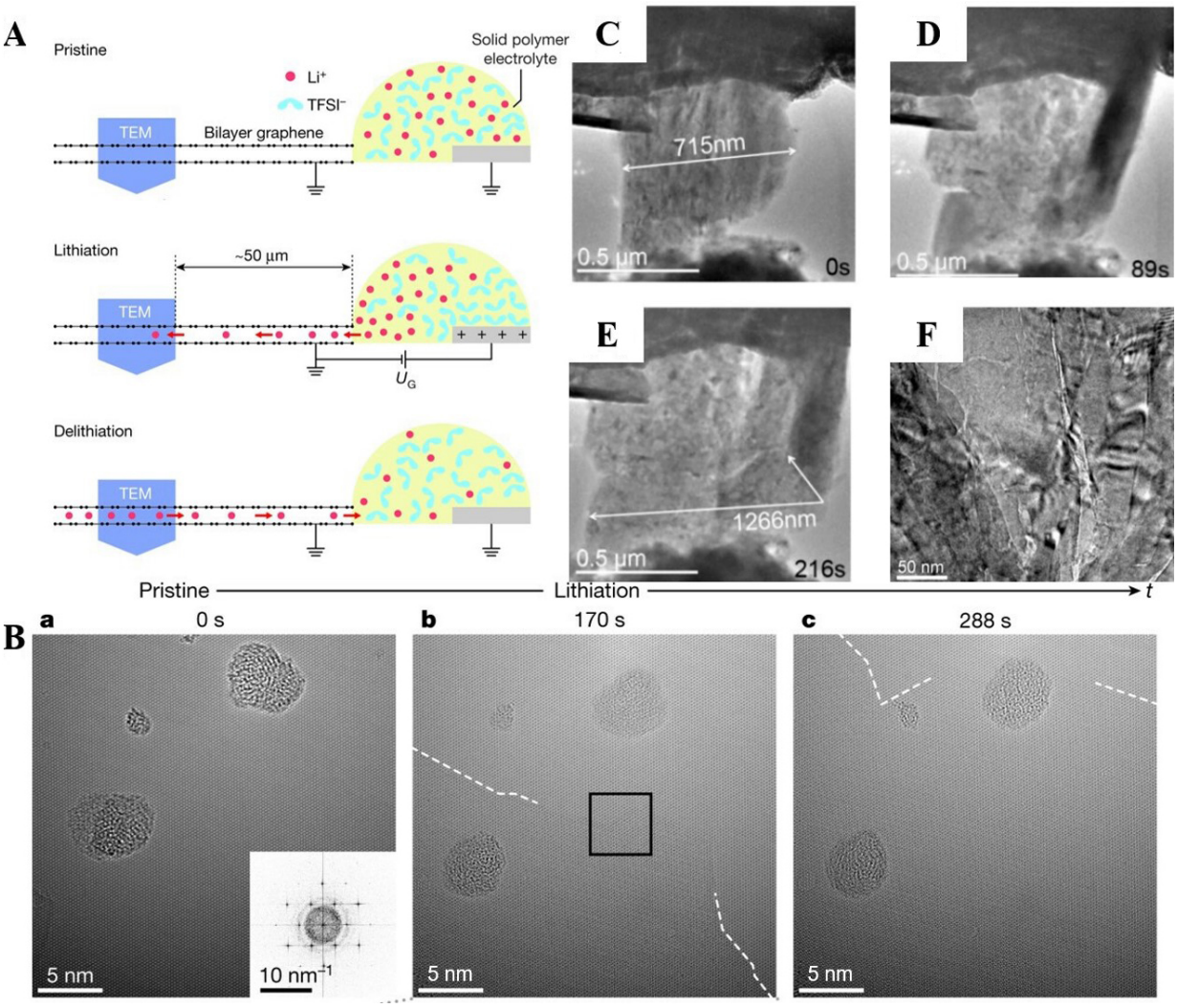

Figure 7. (A) Device layout and working principle. (B) The propagating front (dashed white line) of Li crystal forming inside bilayer graphene during lithiation. Time-resolved TEM images show microstructure evolution of the BP sheet during the first cycle: (C) pristine BP sheet. (D and E) discharging process. The anode cracking and pulverization accompanying the huge size increase appeared in the delithiation process, greatly different from the commonly accepted understanding. (F) Typical magnified TEM image of the delithiated anode, showing obvious cracking. (A and B) are adapted with permission from Ref.[84], copyright 2018, Springer Nature; (C-F) are adapted with permission from Ref.[85], copyright 2016, American Chemical Society.

voltages: pristine BP, Li_3P_7, amorphous LiP, Li_3P and the fully lithiated state at 0.001 V. Both methods showed that the process was fully reversible during the charge process, with BP diffraction peaks appearing again and the absorption edge shifting to higher energy. These operando techniques provide conclusive experimental evidence for the three-step mechanism of lithiation: BP → Li_3P_7 → LiP → Li_3P, and the reverse reaction during delithiation.

APPLICATIONS OF PHOSPHORUS-BASED ANODES IN SOLID-STATE BATTERIES

P is a promising anode candidate for all-solid-state batteries (ASSBs) due to its theoretical capacity of 2,596 mAh g^{-1}, which is nearly seven times higher than that of commercial graphite. Early research utilized mechanical ball milling to form a composite BP with natural graphene and Li_2S-P_2S_5 glass-ceramic electrolytes, achieving an initial discharge capacity of 1,962 mAh g^{-1}, though cycle stability remained a challenge[88]. Recent advancements in synthesis, particularly the vaporization-condensation of RP into zeolite-templated carbon (ZTC), have enabled record-high phosphorus loadings of 65.0 wt%. This P@ZTC

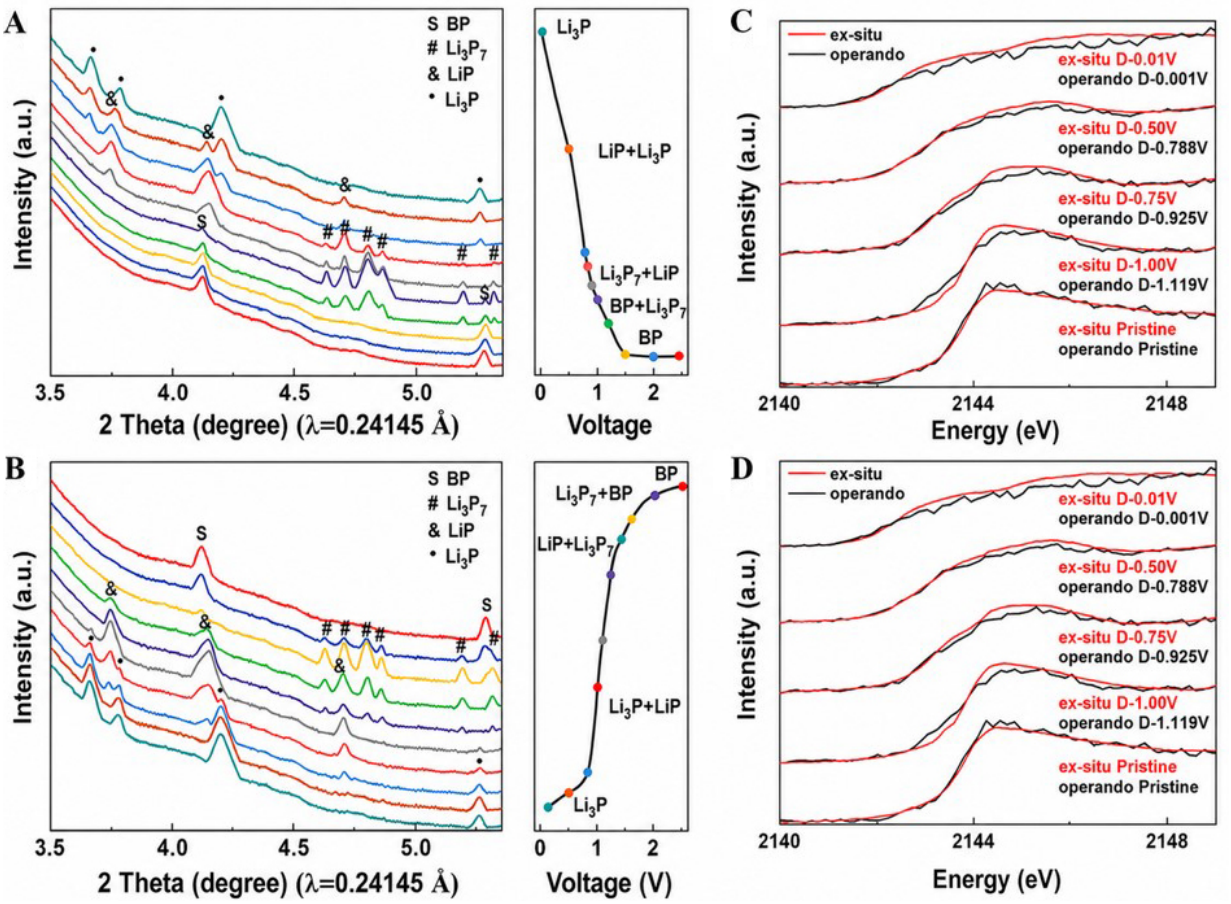

Figure 8. Operando XRD spectra of BP/G/CNTs electrode during (A) discharge (from bottom to top) and (B) charge (from bottom to top). Comparison of *ex situ* and operando P K-edge XAS of BP/G/CNTs of (C) discharge and (D) charge. The figure is adapted with permission from Ref.[87], copyright 2021, Wiley.

composite delivered a high delithiation capacity of 1,823 mAh g^{-1} with an ICE of 87.44% and demonstrated remarkable longevity, maintaining 1,260 mAh g^{-1} after 400 deep discharge-charge cycles[89]. To further optimize high-rate performance, researchers developed electro-mechano-mediation strategies using P/Sb composites. In these systems, an *in-situ* formed Sb/Li Sb phase provides a stiff structural framework and mixed electronic/ionic conductivity, allowing the anode to deliver 340 mAh g^{-1} at an extreme rate of 30 C and retain 64.0% capacity after 10,000 cycles at 10 C[90].

The capacity fading of phosphorus-based ASSBs is a complex process driven by the coupling of interfacial chemical instability and mechanical contact degradation. Unlike liquid electrolytes, rigid SEs cannot flow to wet newly exposed active material surfaces created by the approximately 300% volume expansion of phosphorus during lithiation[91]. Many sulfide electrolytes, including Li_6PS_5Cl, are thermodynamically unstable at the low potentials required for phosphorus lithiation (~0.7 V *vs*. Li^+/Li). These electrolytes undergo irreversible reductive decomposition into Li_3P, Li_2S, and LiCl, forming a high-impedance interphase layer that consumes active lithium and increases cell resistance. This decomposition is often catalyzed by the presence of carbon additives. The lattice breathing of phosphorus during cycling induces significant chemo-mechanical stress that leads to particle cracking and the loss of solid-solid physical contact. This results in electrochemical disconnection, where regions of the active material become isolated and unable to participate in the reaction, forcing the premature termination of charging due to concentration polarization[92].

The degradation mechanisms of phosphorus anodes in solid-state environments differ significantly from those in conventional liquid electrolyte systems. In liquid-based batteries, the primary fading drivers are particle pulverization and the dissolution of intermediate polyphosphides (e.g., LiP_7, Li_3P_7), which shuttle to the cathode and cause rapid active material loss[93]. While liquid electrolytes can wet internal cracks, this benefit is offset by the continuous formation of new SEI layers that consume electrolyte and lithium. Conversely, ASSBs utilize the mechanical rigidity of the solid electrolyte to physically constrain volume expansion and suppress the dissolution of polyphosphides. For example, the thickness increase of a P@ZTC anode was reported as only ~4% in a solid-state cell compared to ~74% in a liquid system after cycling. However, ASSBs are uniquely hindered by point-contact limitations and the irreversible decomposition of the SE into resistive by-products at the interface[89,94]. Overcoming the point-contact limitations and managing the extreme mechanical stress of high-capacity alloying remain the primary challenges for the commercialization of solid-state phosphorus batteries.

CONCLUSION AND OUTLOOK

In this review, we have systematically summarized the significant advancements in phosphorus-carbon composite anodes for LIBs, with a particular focus on how carbon host dimensionality governs electrochemical performance. The key takeaway is clear: no single dimensionality is universally optimal; rather, the choice of carbon architecture must be tailored to the specific failure mechanism-volume expansion, polyphosphide dissolution, or poor conductivity-that dominates for a given phosphorus allotrope and operating condition.

The synthesis of phosphorus-carbon composite anodes for LIBs has established a clear structure-property paradigm in which the dimensionality of the carbon host fundamentally governs lithium storage behavior. 0D QDs minimize ionic diffusion distances but remain prone to aggregation unless covalently anchored, whereas 1D architectures provide continuous percolation pathways but struggle with high phosphorus loading without surface accumulation. 2D heterostructures reduce lithium migration barriers and induce metallic conductivity, albeit at the cost of restacking and low packing density. 3D porous frameworks currently offer the most balanced solution, integrating interior void space for volume accommodation, heteroatom doping for polyphosphide chemisorption, and interconnected networks for rapid transport. Across all dimensional classes, confinement within conductive carbon matrices suppresses pulverization, stabilizes intermediate phases, and limits the dissolution of lithium polyphosphides, while covalent P-C and P-O-C interactions preserve electrical continuity during repeated expansion. Operando characterizations have revealed a multistep phase evolution; yet, the reversibility of intermediate crystalline phases and the conditions favoring amorphous versus crystalline pathways remain poorly understood.

Despite these advances, several critical barriers persist. The intrinsic volume expansion associated with Li_3P formation induces severe mechanical stress and electrode pulverization, with anisotropic expansion in BP causing interlayer slippage and isotropic swelling in amorphous RP proving equally unmitigated by current confinement strategies. The dissolution and shuttle behavior of lithium polyphosphides in conventional carbonate electrolytes accelerate capacity fading, an issue analogous to lithium-sulfur batteries. In solid-state systems, rigid electrolytes cannot wet fractured interfaces, and reductive decomposition of sulfides at phosphorus potentials forms high-impedance interphases, introducing failure modes distinct from liquid cells. Furthermore, most phosphorus-carbon anodes exhibit a phosphorus fraction below 70%, limiting practical energy density, while low intrinsic conductivity and poor ICE remain unresolved. Scalable production is hindered by energy-intensive synthesis, reliance on costly carbon hosts, and sensitivity to ambient atmosphere.

Future research must prioritize five interconnected directions. First, systematic operando studies combining Raman, X-ray diffraction (XRD), and X-ray absorption spectroscopy (XAS) are needed to map phase evolution under realistic fast-charging conditions, particularly the elusive amorphous lithium phosphide intermediates and their role in reversibility. Second, the development of weakly solvating electrolytes or artificial interfacial layers that suppress polyphosphide dissolution while accommodating volume changes is critical for both liquid- and solid-state batteries. Third, engineering composite electrodes with high phosphorus mass loading (> 70 wt%) and high areal capacity (> 3 mAh cm^{-2}) without sacrificing structural integrity must move beyond low-loading proof-of-concept demonstrations. Fourth, the integration of machine learning and high-throughput computational screening into the design of phosphorus-carbon composites represents an emerging frontier. AI-assisted prediction of optimal pore sizes, heteroatom doping configurations, and carbon host morphologies could drastically accelerate the discovery of high-performance compositions. Fifth, scalable and air-tolerant synthesis routes that avoid energy-intensive processing and hazardous intermediates must be prioritized to reduce manufacturing costs and improve sustainability. Biomass-derived carbons, MOF-templated architectures, and low-cost porous hosts provide promising pathways toward environmentally sustainable large-scale production. Among all dimensional classes, 3D porous architectures, particularly those derived from biomass or MOFs, currently show the clearest path toward commercial viability, provided that pore size distribution (optimized in the 2-5 nm range) and surface chemistry (N-doping or P-covalent bonding) are further refined to balance phosphorus confinement with electrolyte infiltration. Addressing these challenges will transform phosphorus-carbon composites from academically intriguing materials into industrially relevant anodes for next-generation high-energy and fast-charging LIBs.

DECLARATIONS

Authors' contributions

Contributed to the conceptual development and supervised the revision of the manuscript: Wang, J.
Wrote the initial draft: Yasin, A.; Chen, Q.
Provided suggestions for revision: Wan, J.; Xu, N.; Peng, P.; Zheng, Z.

Availability of data and materials

Not applicable.

AI and AI-assisted tools statement

During the preparation of this manuscript, ChatGPT (version 5.5, released on 2026-05-05) and Grammarly (version 8.937.0, released 2026-04-21) were used solely for language editing. These tools did not influence the study design, data collection, analysis, interpretation, or the scientific content of the work. All authors take full responsibility for the accuracy, integrity, and final content of the manuscript.

Financial support and sponsorship

This work was financially supported by the National Key R&D Program (Grant No.: 2022YFA1504101) and the Natural Science Foundation of China (Grant No.: 52301296, W2512061, 52261160573), the Beijing Natural Science Foundation (Z230019), the Institute of Process Engineering (IPE) Project for Frontier Basic Research, Grant No. QYJC-2022-008.

Conflicts of interest

All authors declared that there are no conflicts of interest.

Ethical approval and consent to participate

Not applicable.

Consent for publication

Not applicable.

REFERENCES

1. Vinayak, A. K.; Xu, Z.; Li, G.; Wang, X. Current trends in sourcing, recycling, and regeneration of spent lithium-ion batteries—a review. *Renewables* **2023**, *1*, 294-315. DOI
2. Degen, F.; Winter, M.; Bendig, D.; Tübke, J. Energy consumption of current and future production of lithium-ion and post lithium-ion battery cells. *Nat. Energy.* **2023**, *8*, 1284-95. DOI
3. Wei, P.; Wang, H.; Yang, M.; Wang, J.; Wang, D. Relocatable hollow multishelled structure-based membrane enables dendrite-free lithium deposition for ultrastable lithium metal batteries. *Adv. Energy. Mater.* **2024**, *14*, 2400108. DOI
4. Liu, T.; Sun, Y.; Wang, Y.; et al. Architected continuum mixed ionic and electronic conducting alloy negative electrode for fast-charging all-solid-state lithium batteries. *Nat. Commun.* **2025**, *17*, 706. DOI PubMed PMC
5. Xiao, J.; Cai, Z.; Muhmood, T.; Hu, X.; Lin, S.; Hu, X. Tailoring ordered porous carbon embedded with Cu clusters for high-energy and long-lasting phosphorus anode. *Small* **2022**, *18*, 2106930. DOI
6. Yang, S. H.; Kim, J. K.; Jung, D.; Kang, Y. C. Facile fabrication of Si-embedded amorphous carbon@graphitic carbon composite microspheres via spray drying as high-performance lithium-ion battery anodes. *Appl. Surf. Sci.* **2022**, *606*, 154799. DOI
7. Yan, W.; Mu, Z.; Wang, Z.; et al. Hard-carbon-stabilized Li-Si anodes for high-performance all-solid-state Li-ion batteries. *Nat. Energy.* **2023**, *8*, 800-13. DOI
8. Li, Z.; Li, Y.; Bi, C. X.; et al. Construction of organic-rich solid electrolyte interphase for long-cycling lithium-sulfur batteries. *Adv. Funct. Mater.* **2023**, *34*, 2304541. DOI
9. Wang, H.; Wei, P.; Wang, J.; Wang, D. Hollow multishelled structure reviving lithium metal anode for high-energy-density batteries. *Chem. Res. Chin. Univ.* **2024**, *40*, 428-36. DOI
10. Jamouri, Y.; Mwanza, D.; Akhrouf, A.; Chakir, M.; Faik, A. Unlocking the potential of Li-argyrodite solid-state electrolytes: a path toward enhanced Li-ion conduction and electrode-electrolyte compatibility for high-performance next-generation all-solid-state batteries. *Nano. Energy.* **2025**, *144*, 111378. DOI
11. Xu, Z.; Li, H. T.; Cai, N.; et al. Phosphorus-enhanced anodes: a scalable solution to transition-metal ion crosstalk in high-energy lithium-ion batteries. *Angew. Chem. Int. Ed.* **2025**, *138*, e18717. DOI
12. Han, X.; Fang, S.; Pan, J.; Song, S.; Chen, Y.; Sun, J. Beyond the primary solvation sheath: correlating Li^+ solvation sheath structure with the electrochemical performances of phosphorus anode. *J. Energy. Chem.* **2026**, *115*, 412-20. DOI
13. Liu, C.; Han, M.; Cao, Y.; et al. Unlocking the dissolution mechanism of phosphorus anode for lithium-ion batteries. *Energy. Storage. Mater.* **2021**, *37*, 417-23. DOI
14. He, S. A.; Liu, Q.; Cui, Z.; et al. Red phosphorus anchored on nitrogen-doped carbon bubble-carbon nanotube network for highly stable and fast-charging lithium-ion batteries. *Small* **2021**, *18*, 2105866. DOI
15. Smajic, J.; Alazmi, A.; Alzahrani, A.; Emwas, A.; Costa, P. M. The interaction of red phosphorus with supporting carbon additives in lithium-ion battery anodes. *J. Electroanal. Chem.* **2022**, *925*, 116852. DOI
16. Tang, C.; Yu, L.; Jiang, Q.; et al. Polymer-based electrolyte for lithium-based high-energy-density and safe energy storages devices: strategy and mechanisms. *Renewables* **2024**, *2*, 297-340. DOI
17. Dong, S.; Wang, L.; Huang, X.; Liang, J.; He, X. Challenges and prospects of phosphorus-based anode materials for secondary batteries. *Batteries. Supercaps.* **2023**, *6*, e202300265. DOI
18. Zeng, L.; Huang, L.; Zhu, J.; et al. Phosphorus-based materials for high-performance alkaline metal ion batteries: progress and prospect. *Small* **2022**, *18*, 2201808. DOI
19. Sui, Y.; Zhou, J.; Wang, X.; Wu, L.; Zhong, S.; Li, Y. Recent advances in black-phosphorus-based materials for electrochemical energy storage. *Mater. Today.* **2021**, *42*, 117-36. DOI
20. Macdonald, T. J.; Clancy, A. J.; Shutt, R. R.; Howard, C. A. Phosphorene nanoribbons for next-generation energy devices. *Joule* **2022**, *6*, 2441-6. DOI
21. Pan, X.; Rui, K.; Khan, M.; Wang, Q.; Liu, J.; Wang, Y. Recent advances in red phosphorus-carbon composites for lithium/sodium-ion batteries: challenges, synthesis strategies, and prospects. *Electrochim. Acta.* **2025**, *544*, 147570. DOI
22. Cho, T. H.; Chen, Y.; Liao, D. W.; et al. Enabling 6C fast charging of Li-ion batteries at sub-zero temperatures via interface engineering and 3D architectures. *Joule* **2025**, *9*, 101881. DOI
23. Cheng, Z.; Tu, B.; Wu, Y.; Huang, H. High-pressure and high-temperature synthesis of black phosphorus-graphite anode material for lithium-ion batteries. *Electrochim. Acta.* **2024**, *473*, 143510. DOI
24. Ji, C.; Zhou, Q.; Yuan, Y.; et al. Electron-deficient sites on boron-doped graphite enable air-stable and durable red phosphorus anode for lithium-ion batteries. *Energy. Environ. Sci.* **2024**, *17*, 4273-82. DOI

25. Zhang, S.; Liu, C.; Wang, H.; et al. A covalent P-C bond stabilizes red phosphorus in an engineered carbon host for high-performance lithium-ion battery anodes. *ACS. Nano.* **2021**, *15*, 3365-75. DOI
26. Thomas, S. A. Layered two-dimensional black phosphorous-based hybrid electrodes for rechargeable batteries. *J. Energy. Storage.* **2023**, *73*, 109068. DOI
27. Sun, J.; Zheng, G.; Lee, H.; et al. Formation of stable phosphorus-carbon bond for enhanced performance in black phosphorus nanoparticle-graphite composite battery anodes. *Nano. Lett.* **2014**, *14*, 4573-80. DOI
28. Qian, L.; Or, T.; Zheng, Y.; et al. Critical operation strategies toward high-performance lithium metal batteries. *Renewables* **2023**, *1*, 114-41. DOI
29. Zhang, D.; Yuan, T.; Zhang, H.; et al. Research progress of carbon nanotubes as anode materials for lithium-ion batteries: a mini review. *Carbon. Lett.* **2024**, *34*, 2055-79. DOI
30. Li, P.; Jin, H.; Zhong, G.; Ji, H.; Li, Z.; Yang, J. Electrochemistry of P-C bonds in phosphorus-carbon based anode materials. *ACS. Appl. Mater. Interfaces.* **2022**, *14*, 18506-12. DOI
31. Jin, H.; Xin, S.; Chuang, C.; et al. Black phosphorus composites with engineered interfaces for high-rate high-capacity lithium storage. *Science* **2020**, *370*, 192-7. DOI
32. Liang, J.; Hu, Y.; Zhang, K.; et al. 2D layered black arsenic-phosphorus materials: synthesis, properties, and device applications. *Nano. Res.* **2021**, *15*, 3737-52. DOI
33. Park, C. M.; Sohn, H. J. Black phosphorus and its composite for lithium rechargeable batteries. *Adv. Mater.* **2007**, *19*, 2465-8. DOI
34. Cheng, Z.; Chen, P.; Gu, S.; et al. Glucose promoted synthesis of homogeneously embedded black phosphorus carbon composite with enhanced lithium storage performance. *J. Power. Sources.* **2023**, *585*, 233650. DOI
35. Lan, X.; Li, Z.; Zeng, Y.; Han, C.; Peng, J.; Cheng, H. M. Phosphorus-based anodes for fast-charging alkali metal ion batteries. *EcoMat* **2024**, *6*, e12452. DOI
36. Sun, Y.; Wang, L.; Li, Y.; et al. Design of red phosphorus nanostructured electrode for fast-charging lithium-ion batteries with high energy density. *Joule* **2019**, *3*, 1080-93. DOI
37. Wang, L.; Ju, J.; Deng, N.; Cheng, B.; Kang, W. Embedding red phosphorus in hierarchical porous carbon nanofibers as anodes for lithium-ion battery. *Mater. Lett.* **2019**, *240*, 39-43. DOI
38. Cheng, Z.; Wu, Y.; Huang, H. Red phosphorus/graphite composite as a high performance anode for lithium-ion batteries. *Solid. State. Ion.* **2023**, *389*, 116098. DOI
39. Qiu, R.; Ma, D.; Zheng, H.; et al. Performance degradation mechanisms and mitigation strategies of hard carbon anode and solid electrolyte interface for sodium-ion battery. *Nano. Energy.* **2024**, *128*, 109920. DOI
40. Han, X.; Gong, H.; Li, H.; Sun, J. Fast-charging phosphorus-based anodes: promises, challenges, and pathways for improvement. *Chem. Rev.* **2024**, *124*, 6903-51. DOI
41. Zhou, J.; Shi, Q.; Ullah, S.; et al. Phosphorus-based composites as anode materials for advanced alkali metal ion batteries. *Adv. Funct. Mater.* **2020**, *30*, 2004648. DOI
42. Zou, Z.; Yin, M.; Yin, P.; Hu, Z.; Wang, D.; Pu, H. Facile preparation of surface-modified polypropylene nanofiber separators with enhanced ionic transport and welding performance for lithium-ion batteries. *Nano. Energy.* **2024**, *127*, 109774. DOI
43. Wang, T.; Cheng, F.; Zhang, N.; et al. Superassembled red phosphorus nanorod-reduced graphene oxide microflowers as high-performance lithium-ion battery anodes. *Adv. Eng. Mater.* **2021**, *23*, 2001507. DOI
44. Boidi, G.; Ronai, B.; Heift, D.; et al. Tribology of 2D black phosphorus - current state-of-the-art and future potential. *Adv. Colloid. Interface. Sci.* **2024**, *328*, 103180. DOI
45. Sun, Y.; Zeng, F.; Zhu, Y.; Lu, P.; Yang, D. A review on nanoconfinement engineering of red phosphorus for enhanced Li/Na/K-ion storage performances. *J. Energy. Chem.* **2021**, *61*, 531-52. DOI
46. Tian, H.; Wang, H.; Wang, J.; et al. Understanding the intrinsic reactivity of black phosphorus. *Acc. Mater. Res.* **2024**, *5*, 1472-83. DOI
47. Han, X.; Meng, X.; Chen, S.; et al. P-doping a porous carbon host promotes the lithium storage performance of red phosphorus. *ACS. Appl. Mater. Interfaces.* **2023**, *15*, 11713-22. DOI
48. Liu, M.; Li, A.; Lin, H.; et al. Architectural engineering of metal-organic frameworks in lithium-ion batteries: Multifunctional roles, challenges, and future perspectives. *Nano. Energy.* **2025**, *143*, 111310. DOI
49. Liang, X.; Wang, X.; Li, G.; et al. Unlocking the side reaction mechanism of phosphorus anode with binder and the development of a multifunctional binder for enhancing the performance. *J. Power. Sources.* **2022**, *541*, 231686. DOI
50. Li, G.; Ouyang, T.; Xiong, T.; et al. All-carbon-frameworks enabled thick electrode with exceptional high-areal-capacity for Li-Ion storage. *Carbon* **2021**, *174*, 1-9. DOI
51. Yu, W.; Yang, J.; Li, J.; et al. Facile production of phosphorene nanoribbons towards application in lithium metal battery. *Adv. Mater.* **2021**, *33*, 2102083. DOI

52. Rabiei Baboukani, A.; Khakpour, I.; Drozd, V.; Wang, C. Liquid-based exfoliation of black phosphorus into phosphorene and its application for energy storage devices. *Small. Struct.* **2021**, *2*, 2000148. DOI
53. Cheng, Z.; Gong, H.; Gu, S.; et al. Fabrication of a coaxial bilayer bottlebrush-like phosphorus-carbon composite with enhanced lithium storage performance. *J. Energy. Storage.* **2024**, *89*, 111632. DOI
54. Said, S.; Zhang, Z.; Shutt, R. R. C.; et al. Black phosphorus degradation during intercalation and alloying in batteries. *ACS. Nano.* **2023**, *17*, 6220-33. DOI PubMed PMC
55. Puttaswamy, R.; Pai, R. K.; Ghosh, D. Recent progress in quantum dots based nanocomposite electrodes for rechargeable monovalent metal-ion and lithium metal batteries. *J. Mater. Chem. A.* **2022**, *10*, 508-53. DOI
56. Ma, R.; Xiong, L.; Jiao, P.; et al. Origins of severe structural changes during alloying-dealloying reactions in black phosphorus. *J. Am. Chem. Soc.* **2024**, *146*, 23044-53. DOI
57. Jiang, M.; Ma, Y.; Chen, J.; Jiang, W.; Yang, J. Regulating the carbon distribution of anode materials in lithium-ion batteries. *Nanoscale* **2021**, *13*, 3937-47. DOI
58. Pan, L.; Zhu, X.; Sun, K.; Liu, Y.; Xie, X.; Ye, X. Molecular level distribution of black phosphorus quantum dots on nitrogen-doped graphene nanosheets for superior lithium storage. *Nano. Energy.* **2016**, *30*, 347-54. DOI
59. Li, X.; Zhang, S.; Du, J.; et al. Strong interaction between phosphorus and wrinkle carbon sphere promote the performance of phosphorus anode material for lithium-ion batteries. *Nano. Res.* **2023**, *16*, 9273-9. DOI
60. Tong, Z.; Lv, C.; Bai, G. D.; Yin, Z. W.; Zhou, Y.; Li, J. T. A review on applications and challenges of carbon nanotubes in lithium-ion battery. *Carbon. Energy.* **2024**, *7*, e643. DOI
61. Zhao, D.; Yu, J.; Zhang, Y.; Liu, Y.; Guo, S.; Zhang, J. Size-dependent confining effect of phosphorus inside carbon nanotubes for highly stable lithium-ion storage. *ACS. Appl. Nano. Mater.* **2024**, *7*, 1853-62. DOI
62. Li, W.; Yang, Z.; Li, M.; et al. Amorphous red phosphorus embedded in highly ordered mesoporous carbon with superior lithium and sodium storage capacity. *Nano. Lett.* **2016**, *16*, 1546-53. DOI
63. Jiao, X.; Liu, Y.; Li, B.; et al. Amorphous phosphorus-carbon nanotube hybrid anode with ultralong cycle life and high-rate capability for lithium-ion batteries. *Carbon* **2019**, *148*, 518-24. DOI
64. Han, M.; Liang, X.; Han, C.; et al. Cross-linked binary polymeric binder of polyacrylic acid-carboxymethyl cellulose for improving phosphorus anode. *Adv. Funct. Mater.* **2023**, *34*, 2308325. DOI
65. Li, D.; Wang, D.; Rui, K.; et al. Flexible phosphorus doped carbon nanosheets/nanofibers: electrospun preparation and enhanced Li-storage properties as free-standing anodes for lithium ion batteries. *J. Power. Sources.* **2018**, *384*, 27-33. DOI
66. Sun, J.; Liu, C.; Wang, H.; et al. Core-shell structure of a polypyrrole-coated phosphorus/carbon nanotube anode for high-performance lithium-ion batteries. *ACS. Appl. Energy. Mater.* **2021**, *4*, 4112-8. DOI
67. Rojaee, R.; Shahbazian-Yassar, R. Two-dimensional materials to address the lithium battery challenges. *ACS. Nano.* **2020**, *14*, 2628-58. DOI PubMed
68. Jha, B. K.; Yoon, J.; Jang, J. 3D graphene for energy technologies: chemical strategies and industrial challenges. *Acc. Mater. Res.* **2025**, *6*, 799-813. DOI
69. Yang, Z.; Wu, M.; Luo, W.; Liu, G.; Xu, B. Structural, electronic, and transport properties of phosphorene-graphene lateral heterostructure anodes: insights from first-principles calculations. *J. Phys. Chem. C.* **2022**, *126*, 8928-37. DOI
70. Liu, H.; Zou, Y.; Tao, L.; et al. Sandwiched thin-film anode of chemically bonded black phosphorus/graphene hybrid for lithium-ion battery. *Small* **2017**, *13*, 1700758. DOI
71. Sun, L.; Zhang, Y.; Zhang, D.; Zhang, Y. Amorphous red phosphorus nanosheets anchored on graphene layers as high performance anodes for lithium ion batteries. *Nanoscale* **2017**, *9*, 18552-60. DOI
72. Meng, R.; Huang, J.; Feng, Y.; et al. Black phosphorus quantum dot/Ti_3C_2 MXene nanosheet composites for efficient electrochemical lithium/sodium-ion storage. *Adv. Energy. Mater.* **2018**, *8*, 1801514. DOI
73. Wang, H.; Liu, C.; Cao, Y.; et al. Two-dimensional layered green phosphorus as an anode material for Li-ion batteries. *ACS. Appl. Energy. Mater.* **2022**, *5*, 2184-91. DOI
74. Mao, D.; Wang, C.; Li, W.; et al. Hollow multishelled structure: synthesis chemistry and application. *Chem. Res. Chin. Univ.* **2024**, *40*, 346-93. DOI
75. Wei, Y.; Cheng, Y.; Zhao, D.; et al. A universal formation mechanism of hollow multi-shelled structures dominated by concentration waves. *Angew. Chem. Int. Ed.* **2023**, *62*, e202302621. DOI
76. Xu, W.; Bi, R.; Yang, M.; Wang, J.; Yu, R.; Wang, D. Hollow multishelled structural TiN as multi-functional catalytic host for high-performance lithium-sulfur batteries. *Nano. Res.* **2023**, *16*, 12745-52. DOI
77. Hu, Z.; Liu, W.; Xiao, Z.; et al. Catalysis-driven strategy for overcoming kinetic limitations in Sn_4P_3 anodes for lithium-ion storage. *Electrochim. Acta.* **2025**, *523*, 145937. DOI

78. Liu, C.; Yao, J.; Sun, Y.; et al. Ultrafine red phosphorus confined in reasonably designed pitch-based carbon matrix built of well-interconnected carbon nanosheets for high-performance lithium and potassium storage. *Resour. Chem. Mater.* **2024**, *3*, 54-61. DOI
79. Xiao, J.; Lin, S.; Zhang, N.; Hu, X. Hoya-like hierarchical porous architecture as multifunctional phosphorus anode for superior lithium-sodium storage. *ACS. Nano.* **2023**, *17*, 1597-609. DOI
80. Zhou, J.; Liu, X.; Cai, W.; et al. Wet-chemical synthesis of hollow red-phosphorus nanospheres with porous shells as anodes for high-performance lithium-ion and sodium-ion batteries. *Adv. Mater.* **2017**, *29*, 1700214. DOI
81. Kong, W.; Zhao, L.; Guo, J.; et al. Phosphorus decorated MOF-derived microflower-like carbon as a superior anode for lithium-ion batteries. *Carbon* **2023**, *215*, 118439. DOI
82. Xue, J.; Wang, D.; Xia, X.; Chen, Y.; Liu, H. Confined red phosphorus in N-doped hierarchically porous carbon for lithium ion batteries with enhanced rate capability and cycle stability. *Microporous. Mesoporous. Mater.* **2020**, *305*, 110365. DOI
83. Cui, J.; Zhang, J.; Jing, J.; et al. Advances in in situ TEM for dynamic studies of carbon-based anodes in alkali metal-ion batteries. *Adv. Funct. Mater.* **2024**, *35*, 2418059. DOI
84. Kühne, M.; Börrnert, F.; Fecher, S.; et al. Reversible superdense ordering of lithium between two graphene sheets. *Nature* **2018**, *564*, 234-9. DOI
85. Xia, W.; Zhang, Q.; Xu, F.; et al. Visualizing the electrochemical lithiation/delithiation behaviors of black phosphorus by *in situ* transmission electron microscopy. *J. Phys. Chem. C.* **2016**, *120*, 5861-8. DOI
86. El Bendali, A.; Aqil, M.; Hdidou, L.; et al. The electrochemical and structural changes of phosphorus-doped TiO_2 through in situ Raman and in situ X-ray diffraction analysis. *ACS. Omega.* **2024**, *9*, 14911-22. DOI PubMed PMC
87. Li, M.; Li, W.; Hu, Y.; et al. New insights into the high-performance black phosphorus anode for lithium-ion batteries. *Adv. Mater.* **2021**, *33*, 2101259. DOI
88. Ding, H.; Liu, S.; Yang, W.; et al. Electrolyte engineering for phosphorus-based anodes in secondary ion batteries: from liquid solvation to solid-state interface. *Small* **2026**, *22*, e73226. DOI
89. Wang, S.; Liu, D.; Chen, Y.; et al. Optimization of porous structures of carbon matrices for loading red phosphorus to achieve high-capacity and long-life anodes for all-solid-state lithium-ion batteries. *ACS. Appl. Mater. Interfaces.* **2024**, *16*, 38041-52. DOI
90. Shen, K.; Yao, X.; Song, H.; et al. All-solid-state batteries stabilized with electro-mechano-mediated phosphorus anodes. *Energy. Environ. Sci.* **2025**, *18*, 7568-78. DOI
91. Du, Z.; Yang, S.; Liu, X.; et al. Failure mechanisms and fault evolution in all-solid-state batteries: from materials to cell-level degradation. *Battery. Energy.* **2026**, *5*, e70112. DOI
92. Chen, Y.; Yu, H.; Lin, Y.; et al. Revisiting the modification strategies of alloy-base anode for solid-state lithium-ion batteries through deconstructing anode-interface-solid electrolyte. *Nano. Micro. Lett.* **2026**, *18*, 341. DOI PubMed PMC
93. Koerver, R.; Aygün, I.; Leichtweiß, T.; et al. Capacity fade in solid-state batteries: interphase formation and chemomechanical processes in nickel-rich layered oxide cathodes and lithium thiophosphate solid electrolytes. *Chem. Mater.* **2017**, *29*, 5574-82. DOI
94. Furukawa, K.; Yamada, M.; Ariyoshi, K. Quantitative analysis of side-reaction rates and capacity fading mechanisms in all-solid-state Li-ion batteries. *J. Power. Sources.* **2025**, *643*, 237001. DOI